Mineralogical Magazine, August 2017, Vol. 81(4), pp. 781–809

Review

On the nature and origin of garnet in highly-refractory Archean lithospheric mantle: constraints from garnet exsolved in Kaapvaal craton orthopyroxenes

Sally A. Gibson

Department of Earth Sciences, University of Cambridge, Cambridge CB2 3EQ, UK

[*Received 5 August 2016; Accepted 4 October 2016; Associate Editor: Stuart Mills*]

ABSTRACT

The widespread occurrence of pyrope garnet in Archean lithospheric mantle remains one of the 'holy grails' of mantle petrology. Most garnets found in peridotitic mantle equilibrated with incompatible-trace-element-enriched melts or fluids and are the products of metasomatism. Less common are macroscopic intergrowths of pyrope garnet formed by exsolution from orthopyroxene. Spectacular examples of these are preserved in both mantle xenoliths and large, isolated crystals (megacrysts) from the Kaapvaal craton of southern Africa, and provide direct evidence that some garnet in the sub-continental lithospheric mantle formed initially by isochemical rather than metasomatic processes. The orthopyroxene hosts are enstatites and fully equilibrated with their exsolved phases (low-Cr pyrope garnet ± Cr-diopside). Significantly, *P-T* estimates of the post-exsolution orthopyroxenes plot along an unperturbed conductive Kaapvaal craton geotherm and reveal that they were entrained from a large continuous depth interval (85 to 175 km). They therefore represent snapshots of processes operating throughout almost the entire thickness of the sub-cratonic lithospheric mantle.

New rare-earth element (*REE*) analyses show that the exsolved garnets occupy the full spectrum recorded by garnets in mantle peridotites and also diamond inclusions. A key finding is that a few low-temperature exsolved garnets, derived from depths of ~90 km, are more depleted in light rare-earth elements (*LREE*s) than previously observed in any other mantle sample. Importantly, the *REE* patterns of these strongly *LREE*-depleted garnets resemble the hypothetical composition proposed for pre-metasomatic garnets that are thought to pre-date major enrichment events in the sub-continental lithospheric mantle, including those associated with diamond formation. The recalculated compositions of pre-exsolution orthopyroxenes have higher Al_2O_3 and CaO contents than their post-exsolution counterparts and most probably formed as shallow residues of large amounts of adiabatic decompression melting in the spinel-stability field. It is inferred that exsolution of garnet from Kaapvaal orthopyroxenes may have been widespread, and perhaps accompanied cratonization at ~2.9 to 2.75 Ga. Such a process would considerably increase the density and stability of the continental lithosphere.

Keywords: Archean, subcratonic lithospheric mantle, peridotite, garnet, orthopyroxene, Kaapvaal craton.

Introduction

Over the last 50 years our understanding of the thermal and compositional structure of the Earth's interior has changed dramatically. Pivotal to this transformation in scientific understanding have been findings from petrological and geochemical studies on kimberlite-borne mantle xenoliths and inclusions in diamonds; these provide the only direct information on the deep mantle, and in turn unique constraints on its long-term evolution and compositional variability (e.g. Boyd, 1989; Boyd *et al.*, 1993; Burgess and Harte, 2004; Dawson, 2004; Dawson *et al.*, 1980; Harte, 1983; Pearson *et al.*, 2014; Pearson and Wittig, 2013; Stachel *et al.*, 2004, 2005; Walter *et al.*, 2011). Information

E-mail: sally@esc.cam.ac.uk
https://doi.org/10.1180/minmag.2016.080.158

gained from pressure and temperature (*P-T*) estimates of these mantle fragments has been fundamental to calculation of geothermal gradients and calibration of corresponding seismic data, and key to understanding the long wavelength, spatial variability in the thermal structure and thickness of ancient continental lithosphere (e.g. Begg *et al.*, 2009; Griffin *et al.*, 2003; Mather *et al.*, 2011; McKenzie *et al.*, 2005; Priestley and McKenzie, 2013).

Even after several decades of mantle petrology, isotope geochemistry and solid-Earth geophysics there is, however, no consensus on how the ancient cores of continents formed and information on macro-scale geodynamic processes gained from micro-scale observations and *in situ* analyses of individual phases continues to fuel investigations on mantle peridotites. While mantle xenoliths are our only direct probes of the deep Earth, most have suffered modal and cryptic overprinting since their initial time of formation (Boyd *et al.*, 1993; Dawson, 1987), which makes deciphering their pressure-temperature and time histories complex. Much of the interpretation of the compositional evolution of the sub-cratonic mantle has focused on pyrope garnets (e.g. Burgess and Harte, 2004; Gibson *et al.*, 2008, 2013; Harte and Gurney, 1981; Ivanic *et al.*, 2016; Shu and Brey, 2015; Stachel *et al.*, 1998) but the widespread and variable occurrence of this high-density phase in Archean lithospheric mantle remains one of the outstanding 'holy grails' of mantle petrology. The nature and timescales of formation of garnet are important to our understanding of how the deep keels of Earth's sub-cratonic lithospheric mantle have remained stable for the last 2.5 Ga, as it potentially leads to negative buoyancy and destabilization (Gibson *et al.*, 2013; Jordan, 1979; Lee *et al.*, 2011; Peslier *et al.*, 2010; Schutt and Lesher, 2010).

Archean sub-cratonic mantle peridotites are distinguished from those found in off-craton settings by their higher Mg# (Mg/[Mg + Fe] × 100), which is commonly >92, and are considered to be more refractory melt residues (Boyd, 1989). Much of the Archean sub-cratonic lithospheric mantle is thought to consist of amalgamated residues of convecting mantle melting (Boyd *et al.*, 1993; Harte, 1983) that formed by: (1) single-stage melting in a tectonic setting analogous to present-day oceanic spreading ridges (Doucet *et al.*, 2012; Gibson *et al.*, 2008) and/or hotspots (Arndt *et al.*, 2009), but at potential temperatures up to ~250°C higher (Herzberg and Rudnick, 2012; Lee and Chin, 2014; Richter, 1988); or (2) multi-stage shallow melting, initially beneath a spreading ridge followed by hydrous remelting in a convergent tectonic setting (Carlson *et al.*, 2005; Pearson and Wittig, 2008; Shu *et al.*, 2013; Simon *et al.*, 2007). Despite these different opinions on the melting regime, Re-Os model ages indicate that melt depletion events associated with the initial formation of sub-cratonic lithospheric mantle were ancient and occurred between 3.5 and 2.5 Ga (Pearson *et al.*, 1995; Walker *et al.*, 1989). The paradox is that garnet typically occurs in mantle lithologies depleted in clinopyroxene (dunites and harzburgites), which represent residues of major melting events involving up to 40% partial melting, whereas experimental studies on fertile peridotite suggest that garnet should be exhausted by <20% melting (Fig. 1; Herzberg, 2004; Simon *et al.*, 2003; Walter, 1998).

The compositions of pyrope garnets commonly found in mantle peridotite suites are diverse and generally vary in accordance with paragenesis (Burgess and Harte, 2004; Grütter *et al.*, 2004; Gurney *et al.*, 1979; Gurney and Switzer, 1973; Sobolev *et al.*, 1973). For example, garnets from

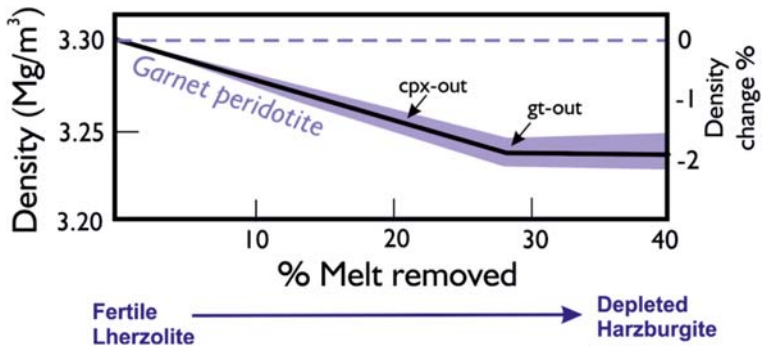

FIG. 1. Change in density of mantle peridotite as garnet is removed during partial melting (after Artemieva, 2011).

harzburgites have low CaO contents and are commonly 'sub-calcic' whereas those found in lherzolites have higher CaO contents, and show a steep positive correlation with Cr_2O_3 (Fig. 2). Typically, pyrope garnets from a lherzolitic sub-cratonic mantle are enriched in strongly-incompatible trace elements from which equilibrium with high-pressure, small-fraction, volatile-rich, metasomatic mantle melts or fluids has been deduced (e.g. Gibson *et al.*, 2013; Shu and Brey, 2015; Stachel and Harris, 1997). A substantial overlap exists between sub-calcic garnets found in harzburgites and those in diamond inclusions (Stachel and Harris, 2008) and suggests that they represent garnets from the early formation of the sub-continental lithosphere. The discovery of: (1) rare garnets with ultra-depleted CaO (<2 wt.%; Fig. 2) and/or very-low incompatible-trace-element contents (Dawson, 2004; Gibson *et al.*, 2013); and (2) exsolution lamellae of garnet in orthopyroxene (Aoki *et al.*, 1980; Dawson, 2004; Dawson *et al.*, 1980; Eggler *et al.*, 1979) suggest that at least some pyrope garnets in the lithospheric mantle have an isochemical rather than a metasomatic origin.

The scarcity of garnets with exceptionally-low CaO is almost certainly because less than 1% of the mantle sampled by xenoliths and megacrysts is unmetasomatized (Pearson and Wittig, 2013) and the extent to which sub-cratonic lithospheric mantle has been affected by exsolution of garnet from orthopyroxene (enstatite) remains enigmatic; much more widely reported is the exsolution of garnet from clinopyroxene in mantle eclogites and pyroxenites rather than peridotites (Beeson and Jackson, 1970; Faryad *et al.*, 2009; Harte and Gurney, 1975; Jerde *et al.*, 1993; Roach, 2004; Sautter and Harte, 1988, 1990; Wilkinson, 1976). Here, I present detailed descriptions of mineral microstructures together with the first *in situ* major- and trace-element analyses of pyrope garnets found as exsolution lamellae in enstatites. Geothermobarometry shows that sub-solidus exsolution occurs over an extensive depth range in the Kaapvaal lithospheric mantle. This supports the hypothesis that isochemical formation of garnet is not a localized feature and hence of importance to our understanding of the evolution and long-term stability of the lithospheric mantle.

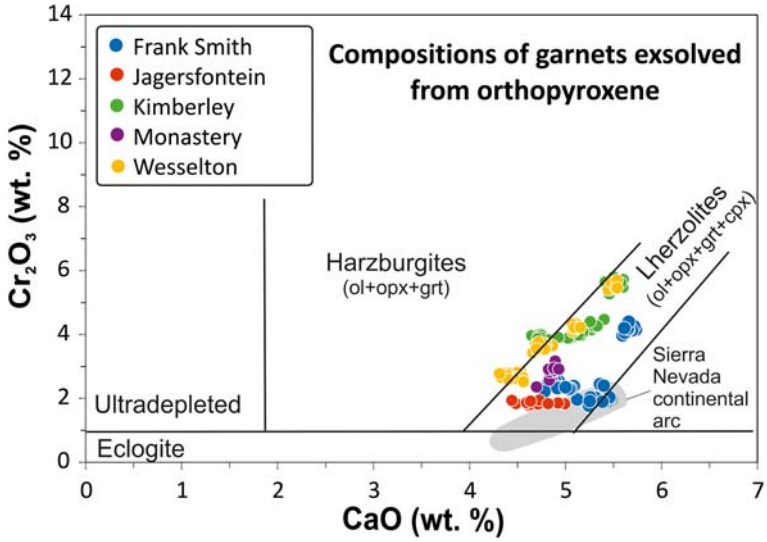

FIG. 2. CaO *vs*. Cr_2O_3 classification plot for mantle garnets in equilibrium with orthopyroxene and/or clinopyroxene, after Sobolev *et al.* (1973) and Grütter *et al.* (2004). The compositions are shown for garnets exsolved in orthopyroxene megacrysts and orthopyroxenes found in mantle peridotites entrained by various kimberlite pipes from the Kaapvaal craton. Garnets in equilibrium with primitive mantle melts are characterized by ~2 wt.% Cr_2O_3 and 4 to 5 wt.% CaO. In garnet lherzolites, orthopyroxene and clinopyroxene buffer the effects of moderate degrees of melt depletion which causes the Ca and Cr contents of garnets to increase until all of the clinopyroxene is exhausted (Grütter *et al.*, 1999; Stachel and Harris, 2008). Data are from Table 2.The field of discrete and exsolved garnets found in peridotites from the Sierra Nevada continental arc (Chin *et al.*, 2012) is shown for comparison (see text for discussion).

Evidence for isochemical formation of pyrope garnet in the lithospheric mantle

Low Ca and Cr ('ultra-depleted') pyrope garnets

Published reports of pyrope garnets formed by isochemical exsolution are abundant in the literature. A small number of pyrope garnets with ultra-depleted major- and/or trace-element compositions have been found in mantle peridotites from the Tanzanian and Kaapvaal cratons (Gibson *et al.*, 2013; Lazarov *et al.*, 2009, 2012; Shu and Brey, 2015), and also in xenocryst suites from the Siberian, North Atlantic and Superior cratons (Grütter and Tuer, 2009; Ziberna *et al.*, 2013). They are distinguished by their very low CaO contents (<2 wt.%; Grütter *et al.*, 2004). Ultra-depleted garnets found in mantle peridotites from the Tanzanian sub-cratonic mantle (at Lashaine) are especially notable because they have very low concentrations of light rare-earth-elements (*LREE*s) that are similar to those of hypothetical garnets thought to have formed prior to metasomatism of the Earth's sub-cratonic mantle (Gibson *et al.*, 2013). These rare Ca- and Cr-poor garnets coexist in chemical and textural equilibrium with highly-refractory olivine ($Fo_{95.4}$) and orthopyroxene (Mg# = 96.4). Importantly, all of these phases are more magnesian than generally encountered in global samples of depleted lithospheric mantle, i.e. harzburgites and diamond inclusion suites (Gibson *et al.*, 2013). The Tanzanian ultra-depleted garnets form interconnecting networks ('necklaces') around grains of orthopyroxene, which together with the major, trace and *REE* contents of the garnets implies an origin by isochemical exsolution involving diffusion of large cations (Si^{4+} and Al^{3+}) to grain boundaries during sub-solidus cooling. The ultra-depleted Tanzanian garnets occur in low-temperature (~1050°C) peridotite xenoliths derived from depths of ~120 km, i.e. shallower than those normally reached by percolating metasomatic melts and fluids in this region, and have not been metasomatized by their transporting melts (Gibson *et al.*, 2013).

Occurrences of garnets with ultra-low CaO contents may be rare because: (1) their low CaO concentrations make them readily susceptible to geochemical overprinting by Ca-rich metasomatic melts (e.g. Burgess and Harte, 2004; Gibson *et al.*, 2013; Griffin *et al.*, 1999*a*; Schulze, 1995); and (2) highly-refractory peridotite is more common in the 'shallow' lithospheric mantle but is not normally brought to the surface by ascending melts, which tend to metasomatize and preferentially sample their source regions in the deeper mantle. Nevertheless, the depleted compositions of these garnets offer important evidence that they are not solely a result of fractional crystallization and/or reaction of percolating, incompatible-trace-element-rich, metasomatic agents in the sub-cratonic lithospheric mantle (Eggler and Wendlandt, 1982; Gurney *et al.*, 1979).

Garnet exsolution from orthopyroxene in megacrysts and peridotite xenoliths from the Kaapvaal sub-cratonic lithosphere

Olivine, orthopyroxene, clinopyroxene, garnet, ilmenite and phlogopite commonly occur as large (>2 cm), single 'megacrysts' in kimberlites (Dawson, 1980). Suites of these mantle megacrysts vary in terms of their compositions and have been divided into: (1) a Cr-poor megacryst suite, which contains garnet, orthopyroxene, clinopyroxene and ilmenite with low Cr_2O_3, high TiO_2 contents and variable Mg# (Harte and Gurney, 1981); and (2) a less-common, Cr-rich megacryst suite with compositions similar to those found in mantle peridotites (Eggler *et al.*, 1979; Moore and Costin, 2016). A further suite of orthopyroxene megacrysts, distinguished by their coarse exsolution lamellae (cf. fine exsolution lamellae present in Cr-poor and Cr-rich orthopyroxene megacrysts) has also been described (Eggler *et al.*, 1979). These orthopyroxene megacrysts are characterized by much lower CaO at a given Al_2O_3 content and extend to more Mg-rich compositions than orthopyroxenes in the Cr-poor and Cr-rich megacryst suites (Gurney *et al.*, 1979).

Chromium-poor megacrysts crystallize over a wide range of temperatures (1050 to 1400°C) in the lower sub-cratonic lithosphere and have been linked via their large size, compositions and ages to fractional crystallization of percolating, metasomatic, kimberlite-like melts (Harte *et al.*, 1993). The sub-microscopic exsolution lamellae in both the Cr-poor and Cr–rich orthopyroxene megacrysts most probably formed by relatively rapid cooling whereas the orthopyroxenes containing macroscopic exsolved garnet are thought to have cooled slowly and represent fragments of ancient lithospheric mantle (Harte and Gurney, 1981). Both fine and coarse garnet exsolution lamellae have been described in orthopyroxene found as megacrysts at Frank Smith and Bellsbank diamond mines in the classic Kimberley area and in a lherzolite xenolith

(BD1366) from Monastery mine, Lesotho (Aoki *et al.*, 1980; Dawson, 2004; Dawson *et al.*, 1980). In the latter, garnet occurs together with Cr-spinel and Cr-diopside as fine-scale exsolution lamellae in a large porphyroclast of orthopyroxene (enstatite) or as a 'necklace' along orthopyroxene grain boundaries (Dawson, 2004). These exsolution textures are associated closely with deformation textures (kink banding) in the enstatite host and appear to be linked to strain of the crystal lattice (Dawson, 1981).

Analytical Methods

In this study, modal proportions of mineral phases were determined by tracing grain boundaries in digital scans and then calculating the areas occupied by each phase using the open-source, image-processing package *Fiji*®. Orthopyroxene, clinopyroxene and garnet were analysed in 13 samples for major and some trace elements using a Cameca SX100 electron microprobe in the Department of Earth Sciences at the University of Cambridge. This was equipped with five wavelength-dispersive spectrometers and one energy-dispersive spectrometer. Trace-element concentrations in garnet were determined in five of these samples using a New Wave UP213 Nd:YAG laser ablation system interfaced to a Perkin-Elmer Elan DRC II inductively coupled plasma mass spectrometer (LA-ICP-MS) in the Department of Earth Sciences at the University of Cambridge. An 80 μm diameter beam and a laser repetition rate of 10 Hz at a power of ~1 mJ (10 J cm^{-2}) were used for the entire study. The spot size was chosen as a compromise between signal intensity and the size of the minerals of interest in the samples. Further details of analytical techniques are provided in Supplementary Files, which have been deposited with the Principal Editor of *Mineralogical Magazine* and are available from http://www.minersoc.org/pages/e_journals/dep_mat_mm.html.

Petrographic description of orthopyroxene and exsolved garnet

This investigation is based on three mantle peridotites and 26 orthopyroxene megacrysts collected in the 1960's by J B Dawson from various kimberlite localities (mines) in central and southern parts of the Kaapvaal craton (Frank Smith, Bultfontein and Wesselton in the Kimberley area, Jagersfontein and Monastery). The orthopyroxene megacrysts occur as euhedral, stout prisms up to several centimetres long. They are fresh and many contain visible crystals of pink-purple garnet and, to a lesser extent, emerald-green clinopyroxene (Fig. 3). Microstructures in the orthopyroxenes – such as undulose extinction and oriented, fine lamellae – are most evident in cross-polarized light (Fig. 4). The textures associated with the exsolved garnet can be subdivided into four types. (1) Fine closely-spaced lamellae or rods. (2) Isolated blebs of exsolved garnet in single grains of orthopyroxene. This texture is the least common. The blebs are elongate and sometimes have spindle shapes with a preferred orientation, parallel to {110} of the host orthopyroxene (e.g. BD1959, Wesselton mine, Fig. 4*a*). (3) Veinlets or chains of rounded grains of pale-pink garnets within orthopyroxene grains. Their orientation varies from parallel, to inclined and/or perpendicular to the cleavage (e.g. BD2015/3a, Frank Smith mine, Fig. 4*b*). (4) Necklace texture formed of equant grains of pale-pink garnet. The interconnected networks of stringers extend over several centimetres along orthopyroxene grain boundaries (e.g. BD1951, Bultfontein mine, Fig. 4*c*). Clinopyroxene also sometimes occurs along grain boundaries in close association with the garnet.

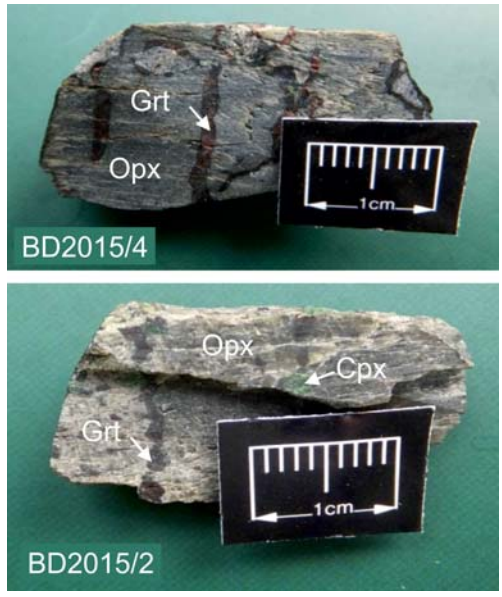

FIG. 3. Hand specimen images of enstatite megacrysts with exsolved pyrope garnet and Cr-diopside.

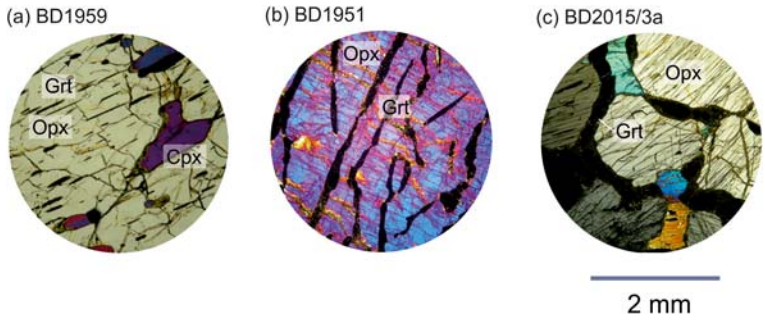

FIG. 4. Photomicrographs (in cross-polarized light) illustrating the range of exsolution textures involving garnet and sometimes clinopyroxene in mantle-derived orthopyroxenes from the Kaapvaal craton. (*a*) Exsolution lamellae of clinopyroxene and blebs of garnet in an orthopyroxene megacryst (BD1959, Wesselton; $P = 39$ kbar, $T = 940$°C); (*b*) exsolution lamellae of garnet in an orthopyroxene megacryst (BD1951, Bultfontein, Kimberley; $P = 37$ kbar, $T = 904$°C); and (*c*) necklace texture of garnet around orthopyroxene in a peridotite xenolith (BD2015/3a, Frank Smith mine; $P = 35$ kbar, $T = 940$°C).

In orthopyroxene megacrysts, garnet tends to be the dominant exsolved phase and may occupy up to ~25 vol.% of the crystal (Table 1). The highest proportion of orthopyroxene occurs in megacrysts that contain isolated blebs of garnet (Fig. 4*a*). Intra-grain exsolution of garnet is best preserved in large orthopyroxene grains (i.e. megacrysts). This is presumably because in the smaller grains (<10 mm), which are commonly found in peridotite xenoliths, diffusion lengths of Al^{3+} and Si^{4+} are such that garnet nucleates in interconnected networks of crystals on orthopyroxene grain boundaries. Clinopyroxene only occurs in small modal amounts (<6%) and forms rods or blebs with deformation twins (Fig. 4*a*). Minor secondary phlogopite was observed in a few samples (Table 1).

Multi-stage, multi-phase exsolution in a single orthopyroxene megacryst

The wide variety of exsolution styles are displayed strikingly in a single enstatite megacryst BD3736/1 (Fig. 5). These offer a unique insight into the sub-solidus cooling history of subcratonic lithosphere and hence are described in detail below.

Megacryst BD3736/1 was entrained by the 86 Ma Jagersfontein kimberlite (Smith *et al.*, 1985). The host enstatite, which is 20 mm long and 10 mm wide and shows undulatory extinction, contains 23% exsolved garnet and 2% exsolved clinopyroxene (Table 1). The exsolved garnets occur as elongate, 1.5 mm wide grains that form evenly-spaced (4 mm) chains parallel to {001} of

TABLE 1. Modal abundances (vol.%) of orthopyroxene host and exsolved phases.

Sample	Locality	Texture	Orthopyroxene	Garnet	Clinopyroxene	Phlogopite
BD1940	Wesselton	Chains	83	17	0	
BD1942	Wesselton	Chains	77	23	0	
BD1945	Wesselton	Necklace	91	9	0	Trace
BD1946	Wesselton	Chains	82	18	0	
BD1951	Kimberley	Chains	82	18	0	Trace
BD1954	Kimberley	Chains	96	1	3	
BD1959	Wesselton	Blebs	93	2	6	
BD2015/2a	Frank Smith	Chains	89	10	1	
BD2015/4	Frank Smith	Chains	84	14	3	
BD2015/5	Frank Smith	Necklace	89	10	1	Trace
BD3736/1	Jagersfontein	Chains	75	23	2	

TABLE 2. Major-element compositions of host orthopyroxenes and exsolved garnets and clinopyroxenes.

LOCALITY	Monastery mine	Monastery mine*	Kimberley			Wesselton				
Sample no.	BD1367 Xenolith	BD1366 Xenolith	BD1954 Megacryst	BD3635 Xenolith	BD1951 Megacryst	BD1959 Megacryst	BD1940 Megacryst	BD1942 Megacryst	BD1945 Megacryst	BD1946 Megacryst
Exsolution texture	Necklace	Necklace	Inclined lamellae	Necklace	Inclined lamellae	Blebs	Inclined lamellae	Inclined lamellae	Necklace	Lamellae/ necklace
Orthopyroxene										
SiO_2	58.16	57.02	57.22	57.21	58.25	57.32	58.18	58.30	58.44	58.32
TiO_2	0.00	0.00	0.02	0.08	0.00	0.08	0.03	0.01	0.01	0.03
Al_2O_3	0.84	0.87	0.75	0.69	0.76	0.73	0.78	0.87	0.71	0.82
Cr_2O_3	0.27	0.27	0.39	0.25	0.26	0.34	0.26	0.21	0.30	0.26
FeOt	4.35	4.22	5.61	7.66	4.33	5.55	4.06	3.89	4.42	4.33
MnO	0.14	0.10	0.13	0.13	0.09	0.15	0.08	0.07	0.08	0.08
MgO	35.40	36.55	34.66	33.20	35.54	34.51	35.91	36.05	35.75	35.75
CaO	0.24	0.25	0.46	0.35	0.37	0.41	0.32	0.36	0.33	0.45
Na_2O	0.10	0.04	0.12	0.10	0.14	0.11	0.10	0.15	0.09	0.13
K_2O	0.02	0.00	0.01	0.01	0.01	0.00	0.01	0.01	0.00	0.00
Total	99.51	99.32	99.38	99.67	99.74	99.21	99.71	99.91	100.13	100.17
Mg#	93.55	93.92	91.67	88.54	93.61	91.72	94.04	94.29	93.51	93.63
Garnet										
SiO_2	42.42	41.72	41.34	41.19	42.16	41.36	42.12	42.60	42.15	42.56
TiO_2	0.00	0.00	0.07	0.17	0.02	0.18	0.05	0.02	0.03	0.11
Al_2O_3	21.77	22.00	19.45	19.77	20.99	19.54	21.34	22.22	20.50	21.90
Cr_2O_3	2.91	2.55	5.52	4.15	4.01	5.63	3.70	2.75	4.26	2.59
FeOt	7.48	7.21	8.59	11.83	6.79	8.55	6.56	6.03	7.04	6.55
MnO	0.48	0.14	0.44	0.47	0.32	0.47	0.34	0.28	0.37	0.32
MgO	20.50	20.96	19.21	17.45	21.16	19.14	21.52	22.10	20.67	21.84
CaO	4.82	4.98	5.47	5.18	4.74	5.47	4.79	4.46	5.10	4.41
Na_2O	0.02	0.01	0.02	0.07	0.03	0.05	0.07	0.04	0.03	0.03
K_2O	0.01	0.00	0.00	0.00	0.02	0.00	0.00	0.01	0.01	0.01
Total	100.42	100.05	100.12	100.27	100.24	100.39	100.48	100.51	100.16	100.31
Mg#	83.00	83.82	79.94	72.45	84.74	79.96	85.39	86.72	83.96	85.59

(continued)

TABLE 2. (*contd*.)

LOCALITY	Monastery mine	Monastery mine*	Kimberley			Wesselton				
Sample no.	BD1367 Xenolith	BD1366 Xenolith	BD1954 Megacryst	BD3635 Xenolith	BD1951 Megacryst	BD1959 Megacryst	BD1940 Megacryst	BD1942 Megacryst	BD1945 Megacryst	BD1946 Megacryst
Exsolution texture	Necklace	Necklace	Inclined lamellae	Necklace	Inclined lamellae	Blebs	Inclined lamellae	Inclined lamellae	Necklace	Lamellae/ necklace
Clinopyroxene										
SiO_2	54.67	53.95	54.47	54.33	-	54.39	-	-	-	-
TiO_2	0.00	0.00	0.06	0.18	-	0.16	-	-	-	-
Al_2O_3	2.83	1.98	1.97	2.73	-	2.35	-	-	-	-
Cr_2O_3	1.77	1.50	2.29	2.13	-	2.39	-	-	-	-
FeOt	1.90	1.43	2.64	3.59	-	2.68	-	-	-	-
MnO	0.05	0.12	0.06	0.10	-	0.12	-	-	-	-
MgO	15.38	17.01	16.17	14.61	-	15.61	-	-	-	-
CaO	20.28	21.86	19.86	18.58	-	19.37	-	-	-	-
Na_2O	2.21	1.46	1.97	2.63	-	2.38	-	-	-	-
K_2O	0.01	0.00	0.02	0.01	-	0.01	-	-	-	-
Total	99.09	99.31	99.52	98.90	-	99.46	-	-	-	-
Mg#	93.52	95.49	91.60	87.87	-	91.22	-	-	-	-
P (kbar) NG85	28.70	29.40	39.75	38.76	36.69	38.65	35.55	31.94	37.44	34.39
T (°C) TA98	789	774	951	914	-	901	-	-	-	-
*T*Ca-in-Opx	763	759	980	908	904	942	870	875	880	940
Depth (km)	95	97	131	128	121	128	117	105	124	113

*Published by Dawson (2004).
** Published by Aoki *et al.* (1980) FS61, BB54 and PHN2367 show disequilibrium.

(continued)

TABLE 2. (*contd*.)

LOCALITY	Frank Smith			Jagersfontein	Bells Bank**	Frank Smith**	Frank Smith**
Sample no.	BD2015/2a	BD2015/4	BD2015/5	BD3736/1	BB54	FS61	PHN2367
Exsolution texture	Megacryst Inclined lamellae	Megacryst Lamellae/necklace	Megacryst Necklace	Megacryst Lamellae/necklace	Megacryst	Megacryst	Megacryst
Orthopyroxene							
SiO_2	57.15	56.47	58.04	58.01	58.09	56.71	57.87
TiO_2	0.11	0.04	0.02	0.01	0.04	0.06	0.05
Al_2O_3	0.55	0.59	0.88	0.71	0.67	0.46	0.55
Cr_2O_3	0.23	0.16	0.26	0.23	0.26	0.34	0.39
FeOt	9.16	10.43	4.52	4.60	5.60	6.90	5.23
MnO	0.14	0.11	0.06	0.08	0.12	0.14	0.15
MgO	32.11	31.80	35.44	35.65	35.09	34.60	35.30
CaO	0.59	0.26	0.22	0.20	0.34	0.58	0.42
Na_2O	0.12	0.07	0.06	0.06	0.40	0.07	0.12
K_2O	0.00	0.00	0.00	0.01	0.00	0.00	0.00
Total	100.17	99.92	99.52	99.55	100.61	99.86	100.08
Mg#	86.20	84.45	93.32	93.25	91.78	89.94	92.32
Garnet							
SiO_2	40.85	40.65	42.53	42.55	41.58	40.35	40.64
TiO_2	0.39	0.07	0.00	0.02	0.20	0.27	0.31
Al_2O_3	19.08	21.45	22.18	22.75	20.37	17.08	16.60
Cr_2O_3	4.40	1.96	2.34	1.86	4.20	8.54	7.88
FeOt	12.80	15.55	7.33	7.91	8.76	9.89	7.92
MnO	0.34	0.52	0.30	0.30	0.42	0.43	0.54
MgO	16.72	15.13	20.49	20.76	19.01	16.78	18.60
CaO	5.66	5.12	4.98	4.60	5.48	7.03	6.36
Na_2O	0.04	0.01	0.02	0.01	0.00	0.03	0.05
K_2O	0.01	0.01	0.01	0.00	0.00	0.00	0.00
Total	100.29	100.48	100.17	100.76	100.02	100.40	98.90
Mg#	69.94	63.43	83.29	82.38	79.45	75.15	80.71

(continued)

TABLE 2. (*contd*.)

LOCALITY	Frank Smith			Jagersfontein	Bells Bank**	Frank Smith**	Frank Smith**
Sample no.	BD2015/2a	BD2015/4	BD2015/5	BD3736/1	BB54	FS61	PHN2367
Exsolution texture	Megacryst Inclined lamellae	Megacryst Lamellae/necklace	Megacryst Necklace	Megacryst Lamellae/necklace	Megacryst	Megacryst	Megacryst
Clinopyroxene							
SiO_2	54.62	54.20	54.81	54.78	54.82	54.67	54.32
TiO_2	0.16	0.09	0.06	0.03	0.20	0.08	0.13
Al_2O_3	1.44	1.70	2.24	2.86	1.63	1.09	1.93
Cr_2O_3	1.10	0.59	1.60	1.75	1.22	1.61	2.92
FeOt	4.47	4.25	1.96	1.44	2.03	2.98	2.48
MnO	0.09	0.06	0.04	0.03	0.12	0.08	0.14
MgO	16.51	15.51	15.64	15.52	16.45	17.53	16.35
CaO	19.73	21.43	20.96	20.95	21.75	21.25	18.12
Na_2O	1.39	1.53	1.91	2.10	1.58	1.09	3.18
K_2O	0.04	0.02	0.00	0.00	0.00	0.07	0.00
Total	99.54	99.38	99.23	99.47	99.80	100.45	99.57
Mg#	86.80	86.68	93.43	95.05	93.52	91.29	92.16
P (kbar) NG85	52.82	30.85	27.49	26.58			
T (°C) TA98	1106	773	762	706			
*T*Ca-in-Opx	1112	797	741	713			
Depth (km)	174	102	91	88			

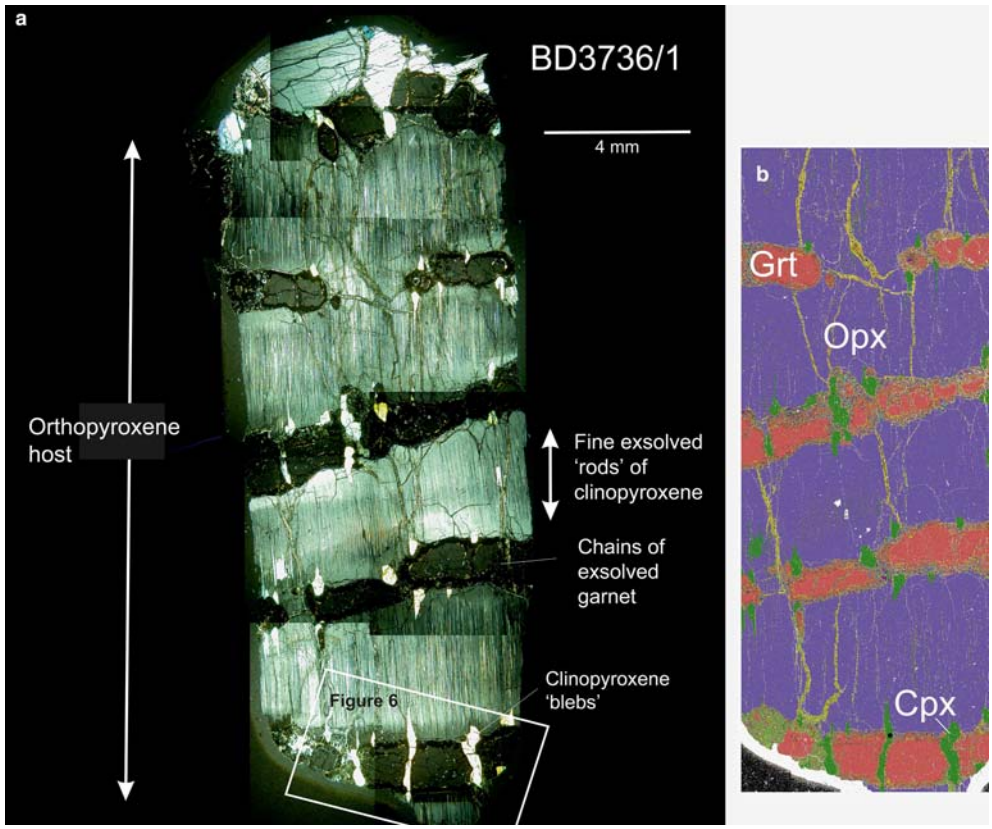

FIG. 5. (*a*) Composite image of orthopyroxene megacryst BD3736/1 (taken in cross-polarized light) illustrating the various styles and length scales of exsolution. (*b*) QEMSCAN® image of orthopyroxene megacryst BD3736/1. Note the different orientations of exsolved pyrope garnet and Cr-diopside. Distance between coarse garnet lamellae is 4 mm.

he orthopyroxene host. Coarse, 'spindle-shaped' blebs and also fine lamellae of clinopyroxene occur perpendicular to the exsolved garnet chains, and are parallel to {110} of the host orthopyroxene (Figs 5 and 6). The clinopyroxene blebs occur at evenly spaced intervals (0.75 mm) along orthopyroxene-garnet grain boundaries and often extend out into the host orthopyroxene forming thin 'tails' (Fig. 6 and Supplementary Figure, deposited at http://www.minersoc.org/pages/e_journals/dep_mat_mm.html). These coarse exsolved clinopyroxenes in some instances cut across the garnet chains. The fine clinopyroxene lamellae are 3.5 mm long and occur at intervals of ~<10 μm. They are best developed away from the chains of exsolved garnet so that ~0.3 mm wide, lamellae-free zones (haloes) occur in the orthopyroxene adjacent to the garnets. Also, at the junction of the garnets and orthopyroxenes there are low-angle, planar, subgrain boundaries that show evidence of dislocation climb. These are variably offset around different garnet grains. Where they occur in dislocation zones, the fine clinopyroxene lamellae show evidence of refraction, usually near their terminations.

Variations in mineral chemistry of host orthopyroxene, exsolved garnet and clinopyroxene

The major-element analyses show that all of the orthopyroxene megacrysts investigated are enstatites (Mg# = 63–94) with low CaO and Al_2O_3 contents and, most importantly, are typical of those found in garnet-bearing mantle peridotites (Fig. 7). At Monastery, Jagersfontein, Bultfontein and

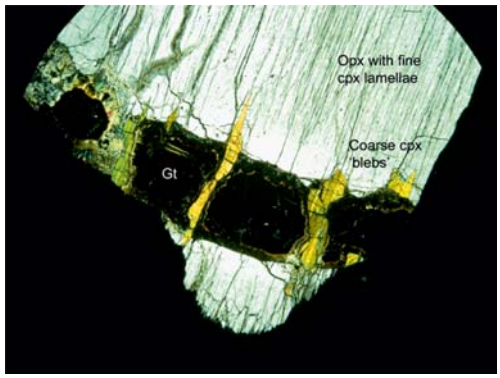

FIG. 6. Photomicrograph showing the relationship between coarse exsolution lamellae of pyrope garnet and spindle-shaped blebs of exsolved Cr-diopside in orthopyroxene megacryst BD3736/1. See Fig. 5 for location of image in relation to whole megacryst.

Wesselton the orthopyroxenes have high Mg# (89 to 94) and Cr_2O_3 (0.21 to 0.4 wt.%), and low but variable contents of both CaO (0.2 to 0.45 wt.%) and Al_2O_3 (0.7 to 0.9 wt.%; Table 2). In BD3736/1 the orthopyroxene host is a high Mg# (93.3), CaO (0.2 wt.%) and Al_2O_3-rich (0.9 wt.%) enstatite (Table 2). A subtle increase (from 0.7 to 0.9 wt.%) in Al_2O_3 was observed in the halo adjacent to the exsolved garnet. Orthopyroxenes from Frank Smith mine are distinctive because of their wide ranges of Mg# (84 to 93), CaO (0.2 to 0.59 wt.%) and Al_2O_3 contents (0.55 to 0.88 wt.%; Table 2).

The exsolved garnets are pyropes with a wide range in Mg# (63 to 87). Whereas garnets in individual samples are compositionally uniform those from different samples have highly variable Cr_2O_3 (1.8 to 5.6 wt.%) but restricted CaO contents (4.4 to 5.7 wt.%) and in these respects resemble mantle garnets of lherzolite paragenesis (Fig. 2). The exsolved garnets in BD3736/1 have a uniform composition and are characterized by high Mg# (82) and TiO_2 (0.02 wt.%). Their CaO (4.6 wt.%) and Cr_2O_3 (1.86 wt.%) contents are among the lowest observed in the Kaapvaal orthopyroxene megacryst suite (Table 2 and Fig. 2). Garnets from Frank Smith mine extend to higher CaO at a given Cr_2O_3 content. All of the exsolved garnets have low

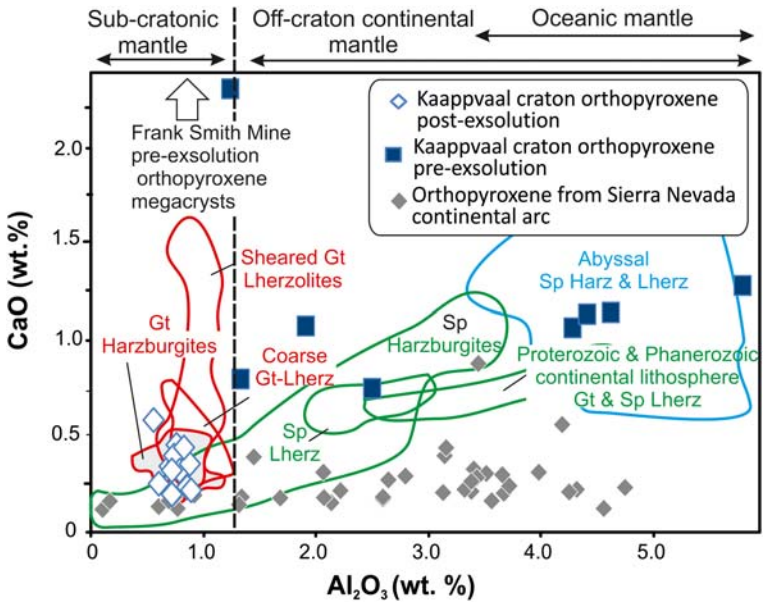

FIG. 7. Al_2O_3 *vs*. CaO contents of mantle orthopyroxenes from different tectonic settings (modified from Gibson *et al.*, 2008). Exsolution of garnet and in some cases clinopyroxene decreases Al_2O_3 and CaO contents so that megacrysts that once had comparable compositions to those found in off-craton spinel lherzolites now resemble those found in on-craton garnet peridotites. Data are from Table 2. Orthopyroxenes found in peridotites from the Sierra Nevada continental arc (Chin *et al.*, 2012) are shown for comparison (see text for discussion).

TiO_2 contents (<0.1 wt.%) and are similar to discrete garnet grains found in lherzolites.

The exsolved clinopyroxenes are characterized by high Ca/(Ca + Mg) ratios (0.45 to 0.50), Mg# (87 to 95) and Cr_2O_3 contents (1.4 to 2.9 wt.%) and are therefore Cr-diopsides (Stephens and Dawson, 1977). The Mg# of the clinopyroxene is usually similar to the orthopyroxene host but Cr_2O_3 contents are much higher. In BD3736/1 the clinopyroxene blebs are more magnesian (Mg# = 95) than the fine clinopyroxene exsolution lamellae (Mg# = 91). The lowest Mg# and Cr_2O_3 contents are found in clinopyroxenes exsolved in orthopyroxene megacrysts from Frank Smith mine. Like the garnets, the clinopyroxenes are characterized by low TiO_2 (<0.2 wt.%), but have moderate Na_2O (1.4 to 2.6 wt.%) and Al_2O_3 contents (1.4 to 2.9 wt.%), and resemble those found in lherzolites.

Given the large variations in major-element contents of the exsolved garnets it is unsurprising that they also show a large range in trace-element concentrations. The highest concentrations of incompatible trace elements (Hf, Sr, Ti, Y and Zr) were found in garnets exsolved from orthopyroxene megacryst BD1959 (Wesselton; Table 3) and in a necklace around an orthopyroxene in peridotite BD3635 (Kimberley). On a chondrite-normalized *REE* plot (Fig. 8), these garnets display a 'normal' pattern, i.e. they have low concentrations of light *REE*s (0.5 to 11 × chondrite) and similar, moderate concentrations of middle to heavy *REE*s (12–20 × chondrite). Garnets from 2015/5 (Frank Smith mine) display mildly-sinusoidal *REE* patterns and have concentrations of light and heavy *REE*s that are much lower than those in BD1959. The different *REE* patterns are not restricted to individual localities, however. At Wesselton exsolved garnets with 'normal' patterns occur together with those that have strongly-sinusoidal chondrite-normalized *REE* patterns (e.g. BD1942). The latter exhibit a maxima at Sm and a minima at Er (Fig. 8). They have low but variable La and Ce concentrations, and the lowest concentrations of heavy rare-earth elements (*HREE*s) out of all of the exsolved garnets analysed. Exsolved garnets in orthopyroxene megacryst BD3736/1 (Jagersfontein) are especially notable because they have extremely-low concentrations of Hf, Nb, Pb, Rb, Th, U, Zr and *LREE*s, which are typically below detection limits (Table 3). Concentrations of *LREEs* are <0.04 × chondrite and *HREEs* are up to 10 × chondrite. As a consequence, garnets from BD3736/1 have very steep slopes on normalized *REE* plots (Fig. 8).

Reconstructed primary orthopyroxene compositions

The reconstructed bulk compositions of pre-exsolution Kaapvaal orthopyroxene megacrysts are shown in Table 4. These are calculated from the major-element compositions and modal proportions of both the exsolved and host phases (Tables 1 and 2). The pre-exsolution megacryst compositions all have the correct stoichiometry for orthopyroxene but they are highly variable in terms of Mg# (84 to 93.5), Al_2O_3 (0.8 to 5.8 wt.%) and CaO contents (0.8 to 5.6 wt.%). It is noteworthy that the Mg# of both the reconstructed pre-exsolution orthopyroxene (Table 4) and post-exsolution orthopyroxene megacrysts (Table 1) are similar and do not appear to have changed during exsolution. This is consistent with the findings of von Seckendorff and O'Neill (1993) which showed that the Fe/Mg ratio in orthopyroxene is controlled by bulk-rock composition and relatively insensitive to changes in temperature and pressure. In contrast to Mg#, the contents of both CaO and Al_2O_3 are noticeably greater (Fig. 7) and the SiO_2 content is lower in the pre-exsolution orthopyroxene.

Final *P-T* estimates for Kaapvaal orthopyroxene megacrysts and mantle peridotites

The presence of co-existing orthopyroxene, garnet and sometimes clinopyroxene allows final equilibration pressures and temperatures (i.e. post exsolution) of the Kaapvaal megacrysts and peridotite xenoliths to be estimated. Combinations of the two-pyroxene solvus thermometer of Taylor (1998), the Ca-in-orthopyroxene thermometer of Brey and Köhler (1990) and the garnet-orthopyroxene Al-barometer of Nickel and Green (1985) were used iteratively to estimate temperatures and pressures, as recommended by Nimis and Grütter (2009). These geothermometers and geobarometers rely on major-element contents of various co-existing minerals and assume that the phases are fully equilibrated. The extent of equilibrium in co-existing mineral phases was established following the recommendations of Nimis and Grütter (2009). An initial check was made by comparing temperatures estimated for samples bearing both clinopyroxene and orthopyroxene. These showed only a slight difference (<30° C) for the two-pyroxene solvus (Taylor, 1998) and Ca-in-orthopyroxene thermometers (Brey and Kohler, 1990; Fig. 9). Some of the samples from

TABLE 3. Trace and rare-earth element abundances in exsolved garnets determined by LA-ICP-MS.

	BD1942 ('Sinusoidal')			BD1959 ('Normal')				BD2015/5 ('Mildly sinusoidal')	
Element	g1-g4	g5-7	g8-10	g1-4	g5-7	g8-9	g10-11	g4-6	g7-9
Sc	74.5	77.2	80.8	183.1	176.0	217.1	186.9	91.0	102.4
Ti	115	137	164	961	871	1063	880	180	165
V	190	189	197	143	139	157	149	110	153
Ni	51.0	40.4	47.2	51.9	33.6	157.1	44.0	30.6	42.2
Rb	0.77	-	-	2.05	0.83	8.71	0.60	-	-
Sr	5.47	1.86	1.04	6.53	2.49	10.91	4.72	-	0.52
Y	2.37	2.14	2.27	17.59	16.65	20.51	18.63	4.24	7.93
Zr	41.2	48.9	42.4	74.4	70.6	84.6	64.2	5.25	9.96
Nb	0.69	0.46	0.24	0.28	0.17	0.21	0.26	-	0.36
Ba	4.00	1.18	2.31	12.05	0.11	2.27	0.51	0.63	-
La	0.42	0.10	0.05	0.29	0.11	0.38	0.27	0.02	0.10
Ce	1.07	0.53	0.27	2.40	2.43	2.58	2.57	0.30	0.39
Pr	0.28	0.21	0.19	0.99	1.11	0.99	1.05	0.10	0.16
Nd	2.86	3.41	3.26	8.75	8.29	8.64	8.37	0.66	1.44
Sm	1.87	1.88	2.17	2.86	3.11	3.02	3.12	0.41	1.08
Eu	0.59	0.60	0.63	1.22	1.11	1.22	1.20	0.17	0.51
Gd	1.51	1.50	1.73	3.81	3.87	4.45	3.82	0.83	1.35
Tb	0.14	0.13	0.15	0.58	0.58	0.72	0.61	0.11	0.31
Dy	0.53	0.49	0.51	3.56	3.41	4.39	3.76	0.64	1.61
Ho	0.07	0.09	0.11	0.70	0.72	0.83	0.77	0.16	0.23
Er	0.25	0.22	0.27	2.21	1.75	2.44	2.04	0.39	0.63
Tm	0.05	0.05	0.06	0.31	0.24	0.32	0.29	0.06	0.07
Yb	0.45	0.52	0.47	2.11	1.81	2.50	2.06	0.55	0.65
Lu	0.09	0.09	0.09	0.34	0.33	0.37	0.35	0.10	0.13
Hf	0.64	0.74	0.75	1.40	1.45	1.52	1.46	0.09	0.08
Ta	0.04	-	0.02	0.03	0.27	0.01	0.18	0.01	0.02
Pb	0.13	0.08	0.07	0.16	0.18	0.28	0.15	0.43	0.16
Th	0.06	0.04	0.03	0.03	0.04	0.04	0.04	0.01	0.00
U	0.10	0.07	0.42	0.08	0.13	0.05	0.14	0.02	0.03

	BD3635 ('Normal')				BD3736/1 ('Depleted')							
Element	gt_1_3	gt_4_6	gt_7_9	gt_10_12	gt_1_3	gt_4_6	gt_7_9	gt_10_12	gt_13_15	gt_16_18	gt_19_21	gt_22_24
Sc	131	143	158	148	73.5	73.5	67.4	67.1	66.4	58.3	74.5	68.7
Ti	914	936	1041	995	119	108	195	172	110	114	123	123
V	146	155	180	173	130	166	213	197	124	145	152	140
Ni	43.01	34.58	39.89	35.10	35.6	38.8	34.4	31.8	34.9	30.0	58.2	33.6
Rb	0.08	-	0.11	0.02	b.d	b.d	b.d	0.092	b.d	b.d	0.084	b.d
Sr	0.42	0.44	2.73	0.40	0.435	b.d	b.d	0.328	b.d	b.d	b.d	b.d
Y	19.40	22.93	30.51	20.47	3.90	4.41	4.60	4.47	4.52	4.21	4.34	4.17
Zr	69.3	76.5	92.8	80.9	b.d	b.d	0.197	0.169	b.d	b.d	0.136	0.150
Nb	0.168	0.178	0.341	0.169	0.050	b.d	0.030	0.032	0.032	0.032	b.d	b.d
Ba	0.346	0.037	1.851	0.057	b.d	0.548	b.d	1.130	0.825	0.013	1.138	0.045
La	0.030	0.021	0.254	0.022	b.d	0.003	0.004	0.003	0.003	0.002	0.005	0.003
Ce	0.354	0.336	0.783	0.422	b.d	0.006	0.004	0.003	0.015	0.004	0.012	0.005
Pr	0.183	0.181	0.247	0.217	0.002	0.004	0.003	0.002	0.002	0.001	0.001	0.002
Nd	2.273	2.360	2.600	2.710	0.023	0.008	0.018	0.018	0.012	0.016	0.018	0.022
Sm	2.123	2.123	2.483	2.303	0.025	0.018	0.025	0.020	0.012	0.021	0.018	b.d
Eu	0.978	1.070	1.217	1.106	0.009	0.016	0.015	0.016	0.012	0.014	0.014	b.d
Gd	3.310	3.657	4.570	3.827	0.082	0.104	0.106	0.099	0.067	0.081	0.088	0.087
Tb	0.554	0.629	0.800	0.605	0.033	0.043	0.034	0.038	0.037	0.036	0.038	0.037
Dy	3.093	3.763	4.940	3.357	0.398	0.428	0.445	0.455	0.474	0.445	0.450	0.408
Ho	0.663	0.796	1.074	0.715	0.133	0.146	0.152	0.150	0.146	0.135	0.144	0.135
Er	1.887	2.253	3.090	2.043	0.570	0.627	0.671	0.630	0.644	0.613	0.590	0.595
Tm	0.291	0.351	0.458	0.323	0.101	0.110	0.115	0.125	0.110	0.105	0.105	0.106
Yb	2.083	2.433	3.113	2.213	0.843	0.980	1.037	0.967	0.980	0.927	0.993	0.917
Lu	0.371	0.423	0.546	0.402	0.152	0.169	0.165	0.170	0.167	0.161	0.159	0.150
Hf	0.739	0.821	0.901	0.861	b.d	b.d	0.013	b.d	0.009	b.d	0.011	b.d
Ta	0.008	0.010	0.019	0.008	b.d	b.d	b.d	0.002	b.d	b.d	b.d	b.d
Pb	0.114	0.043	0.058	0.034	b.d	0.104	0.080	0.084	0.042	0.035	b.d	0.070
Th	0.007	0.004	0.046	0.002	b.d	b.d	b.d	0.002	0.002	b.d	0.003	0.003
U	0.016	0.019	0.022	0.013	b.d	b.d	0.006	0.005	b.d	0.005	b.d	0.012

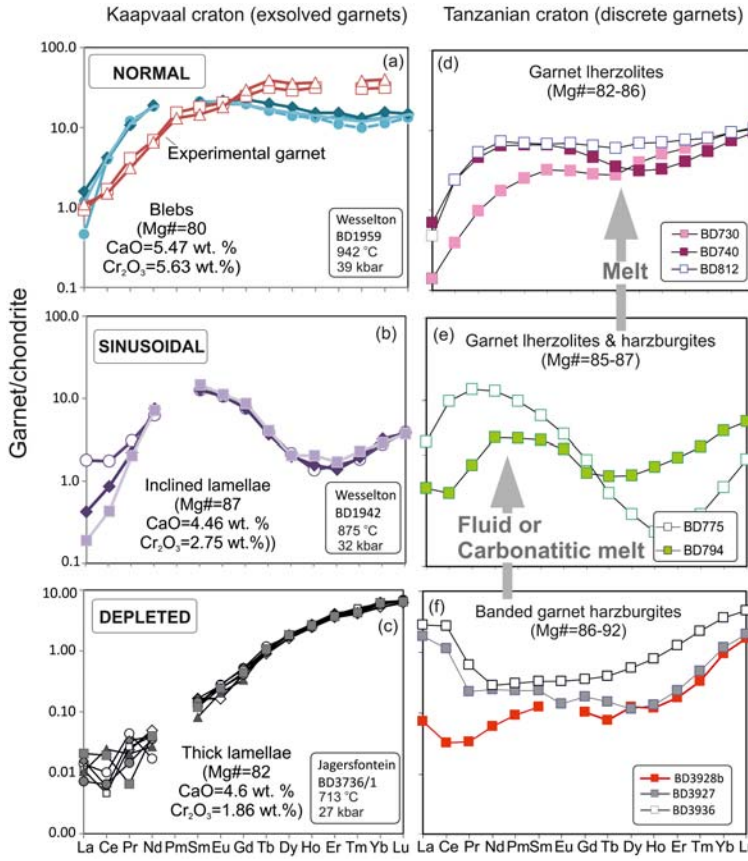

FIG. 8. Chondrite-normalized rare-earth-element plots illustrating the range of compositions of garnets exsolved from orthopyroxene found in Kaapvaal mantle megacrysts and peridotites. The various rare-earth-element patterns displayed by garnets found in mantle peridotites from the Tanzanian craton (Gibson *et al.*, 2013) are shown for comparison as are the compositions of garnets in equilibrium with convecting mantle melts (Tuff and Gibson, 2006). Data are from Table 3. Chondrite normalization factors are from McDonough and Sun (1995).

Jagersfontein, Frank Smith and Monastery equilibrated at temperatures outside the lower bound of experiments used by Taylor (1998), i.e. <900°C. Brey and Kohler (1990) showed that at these low temperatures the Ca-in orthopyroxene parameterization gives slightly high values but the excellent positive correlation between the results from the two thermometers ($R^2 = 0.968$) confirms that the orthopyroxene and exsolved clinopyroxene are fully equilibrated. The temperatures obtained for both clinopyroxene-bearing and clinopyroxene-free samples are therefore internally consistent regardless of the parameterization used.

Pressure estimates for Kaapvaal samples containing fully-equilibrated orthopyroxene and exsolved garnet range from 26 to 53 kbars, which correspond to a depth interval of 85 to 175 km in the lithosphere. Temperature estimates for the same samples are also highly variable, ranging from 700 to 1100°C (Table 2 and Fig. 10). Importantly, Fig. 10 shows that co-variations in temperature and pressure recorded by these samples correspond almost exactly to the 45.6 mW/m^2 conductive geotherm for kimberlite-hosted mantle peridotites from Finsch mine in the western Kaapvaal craton (Gibson *et al.*, 2008; Lazarov *et al.*, 2009). Xenoliths from the 118 Ma Finsch kimberlite (Smith *et al.*, 1985) were entrained over a large depth interval and define a geotherm that is less perturbed at the base of the lithosphere than those hosted by some more recent Kaapvaal kimberlites, which are thought to be affected by regional heating

TABLE 4. Calculated composition of orthopyroxene megacryst prior to exsolution.

Garnet and clinopyroxene microstructures	BD1940 Inclined lamellae	BD1942 Inclined lamellae	BD1945 Necklace	BD1946 Lamellae/ necklace	BD1951 Inclined lamellae	BD1954 Necklace	BD1959 Blebs	BD2015/2a Inclined lamellae	BD2015/4 Lamellae/ necklace	BD2015/5 Necklace	BD3736/1 Lamellae/ necklace
SiO_2	55.45	54.69	56.98	55.48	55.35	56.72	56.88	56.74	56.24	57.56	56.95
TiO_2	0.03	0.01	0.01	0.05	0.01	0.03	0.08	0.12	0.05	0.03	0.02
Al_2O_3	4.27	5.78	2.49	4.61	4.40	1.32	1.90	0.82	1.38	1.23	1.64
FeO	4.48	4.38	4.65	4.73	4.77	5.67	5.73	8.73	9.82	4.29	3.94
MnO	0.12	0.12	0.11	0.12	0.13	0.13	0.17	0.14	0.12	0.06	0.07
MgO	33.47	32.84	34.39	33.24	32.95	34.01	33.56	30.40	29.34	33.31	30.73
CaO	1.08	1.30	0.76	1.16	1.15	0.81	1.09	2.56	3.37	2.34	5.06
Na_2O	0.09	0.12	0.08	0.11	0.12	0.14	0.16	0.24	0.27	0.25	0.53
Total	98.99	99.24	99.47	99.50	98.88	98.83	99.57	99.75	100.59	99.07	98.94
Mg#	93.01	93.04	92.95	92.61	92.49	91.44	91.26	86.12	84.19	93.26	93.29
T_F(°C)	870	875	880	940	904	980	942	1112	797	741	713
P_F (kbar)	35.55	31.94	37.44	34.39	36.69	39.75	38.65	52.82	30.85	27.49	26.58
$T_{solidus}$ at P_F	1529	1493	1547	1517	1540	1568	1558	1680	1482	1447	1438
ΔT (°C)	659	618	667	577	636	588	616	568	685	706	725

T_F(°C) is the final equilibration temperature and, for internal consistency, was calculated using the TCa-in-opx thermometer of Nimis and Grutter (2009).
P_F (kbar) is the final equilibration pressure.
$T_{\text{Anhydrous peridotite solidus}} = -1.092(P-10)^2 + 32.39(P-10) + 1935$, where P is in GPa and T in °C (Hirschmann *et al.*, 2000).
ΔT (°C) is the temperature difference between the solidus and P_F.

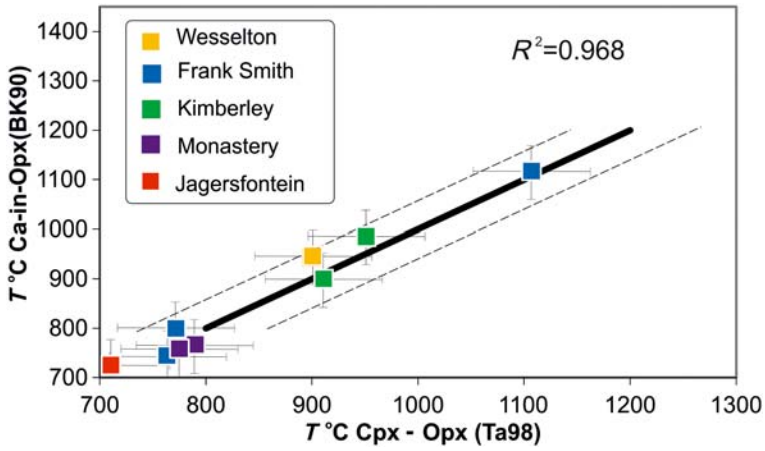

FIG. 9. Comparison of equilibration temperatures estimated for orthopyroxene megacrysts using the two-pyroxene solvus thermometer of Taylor (1998) and the Ca-in-orthopyroxene thermometer of Brey and Kohler (1990). Dashed lines are 60°C tolerance limits from a 1:1 correlation (thick solid line) of the thermometers as suggested by Nimis and Grütter (2009). *P-T* data are from Table 2.

events (Bell *et al.*, 2003). Pressure-temperature estimates from Finsch suggest that the base of the mechanical boundary layer beneath the Kaapvaal craton is at a depth of ~204 km (Fig. 10). The deepest orthopyroxenes exhibiting exsolution of garnet that were examined in this study were therefore entrained from within 30 km of this major boundary.

Discussion

The orthopyroxenes with exsolved garnet that were examined in this study are remarkably fresh and offer a new perspective on the garnet paradox. The lack of any signs of dissolution of the megacrysts is somewhat surprising, given the susceptibility of orthopyroxenes to react with silica-undersaturated melts during transport to the surface (Bussweiler *et al.*, 2016; Russell *et al.*, 2012; Soltys *et al.*, 2016), and the extent to which the orthopyroxenes have interacted with the host kimberlite is limited. While thin veins that cross-cut the exsolved garnets in the orthopyroxene megacrysts may be evidence of post-entrainment interaction and kimberlite infiltration, the variability in enrichment of the *LREE*s in the exsolved garnets appears to be depth dependent, i.e. occurred prior to entrainment, such as at Wesselton where a variety of different styles of *REE* enrichment is evident (Fig. 8).

What are the crystal controls on garnet exsolution from orthopyroxene?

The results of the high temperature (1450 to 1525°C) and pressure (<4.5 to 5.5 GPa) experiments of Canil (1991) suggest that both garnet and clinopyroxene might form in the lithospheric mantle as a result of sub-solidus isochemical exsolution from orthopyroxene. It is anticipated that the size and spacing of the exsolved garnets will vary systematically according to diffusion mechanisms and decrease with the rate of sub-solidus cooling. Greater insights into this process are provided by enstatite-rich megacryst BD3736/1, which records the variable length scales of diffusion that accompanies sub-solidus cooling and exsolution (see above).

The multi-stage exsolution involved in the cooling of this megacryst is interpreted as follows: (1) At high sub-solidus temperatures enstatite with high contents of CaO and Al_2O_3 behaves as a monoclinic crystal (clino-enstatite) and exsolves pyrope garnet parallel to {001}. Equant 2–3 mm grains of garnet coalesce into widely-spaced chains. (2) Sub-solidus exsolution and diffusion of large cations (Ca^{2+}, Al^{3+} and Si^{4+}) causes clino-enstatite to invert to ortho-enstatite, perhaps promoting deformation of the crystal lattice. (3) This exsolution of clinopyroxene (Mg# = 95) and nucleation occurs as equally-spaced 'spindle-shaped' blebs along orthopyroxene-garnet grain boundaries and parallel to {110} (Fig. 6). (4) This nucleation and growth of coarse

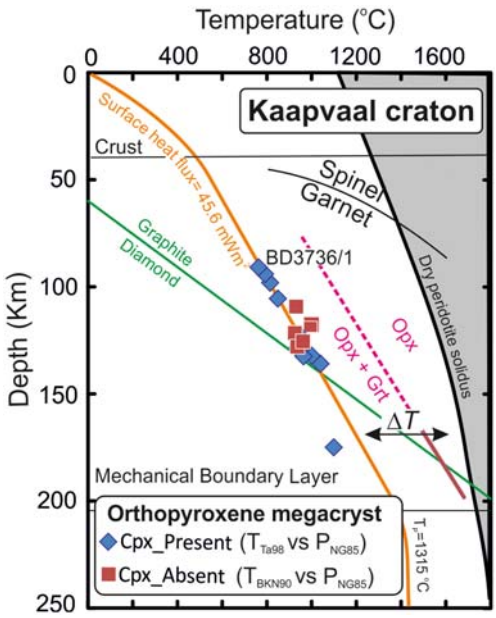

FIG. 10. Temperature *vs*. depth profile through the Kaapvaal craton. The conductive geotherm is calculated using the *P-T* estimates for Finsch peridotites (data from Gibson *et al.*, 2008; Lazarov *et al.*, 2009), a crustal thickness of 38 km (Nair *et al.*, 2006) and an ambient mantle potential temperature of 1315°C in the program *FITPLOT* (McKenzie *et al.*, 2005). *P-T* estimates for Finsch peridotites are from the same geothermometers and geobarometers as the orthopyroxene megacrysts, i.e. the formulations of Taylor (1998), Brey *et al.* (1990) and Nickel and Green (1985). *P-T* data are from Table 2. ΔT is the difference in temperature of the anhydrous peridotite solidus (Hirschmann, 2000) and the conductive geotherm at a given pressure. The stability fields of graphite and diamond, and orthopyroxene and garnet, are from Kennedy and Kennedy (1976) and Canil (1991), respectively. The spinel-garnet transition is from Klemme and O'Neill (2000). See text for discussion of exsolution textures in BD3736/1.

garnet and clinopyroxene creates depletion 'haloes' in the host orthopyroxene (Fig. 6). (5) Homogeneous nucleation and crystallization of clinopyroxene takes place away from the depletion 'haloes' associated with previously exsolved garnet and clinopyroxene, to form equally-spaced fine lamellae (Mg# = 91) parallel to {110}. (6) Finally, dislocation creep results in planar, sub-grain boundaries parallel to garnet-orthopyroxene grain boundaries.

Isochemical exsolution of garnet from orthopyroxene during lithospheric cooling

A key finding from the thermobarometry is that garnet is exsolving from orthopyroxene throughout most of the depth range where garnet is stable (85–175 km) in the Kaapvaal lithospheric mantle, which implies that this is not a localized process. In this study, evidence that some of the exsolved garnets have interacted with percolating metasomatic fluids and melts is provided by their rare-earth-element patterns. It can be seen from Fig. 8 that the 'normal' and 'sinusoidal' *REE* patterns displayed by the exsolved garnets resemble those exhibited by global garnets of lherzolitic and harzburgitic paragenesis, respectively. A significant observation from this study is that garnet and clinopyroxene most highly-depleted in strongly-incompatible trace-element concentrations were exsolved from orthopyroxene megacrysts entrained from the shallowest depths (~90 km) and lowest temperatures (~700°C; Fig. 8). While this is most profound for Jagersfontein megacryst BD3736/1, garnets with low Cr_2O_3 (<3 wt.%) and *REE* abundances are also found exsolved in fully-equilibrated orthopyroxene megacrysts that were entrained from shallow depths in the lithospheric mantle beneath Wesselton and Frank Smith mines.

The low concentrations of trace elements that characterize some of the exsolved garnets (e.g. BD3736/1, Table 3) are highly significant because they are similar to the hypothetical composition proposed for mantle garnets prior to metasomatism by fluids and small-fraction kimberlite-like melts (Shu and Brey, 2015; Stachel *et al.*, 2004; Ziberna *et al.*, 2013; Fig. 11*a*). The *HREE* contents of the hypothetical compositions were estimated from the Dy to Lu slope on chondrite-normalized *REE* plots of sub-calcic garnets whereas the light and middle *REE*s (La to Tb) were calculated from experimental melt partition coefficients (e.g. Johnson, 1998). A further important finding is that the most *LREE*-depleted exsolved garnets have even lower concentrations of La, Ce, Pr and Nd than the most *LREE*-depleted garnets found to date in both peridotite xenoliths (from Tanzania; Gibson *et al.*, 2013) and diamond inclusion suites, e.g. from Kankan and Yakutia (Stachel *et al.*, 2000; Taylor *et al.*, 2003); Fig. 11*b*, *c*, *d*). The latter is significant because once having been encapsulated by diamonds, garnets are protected from later metasomatic events (Shu and Brey, 2015) and their *REE* patterns reveal enrichment that may pre-date or coincide with diamond formation (Fig. 11*e*).

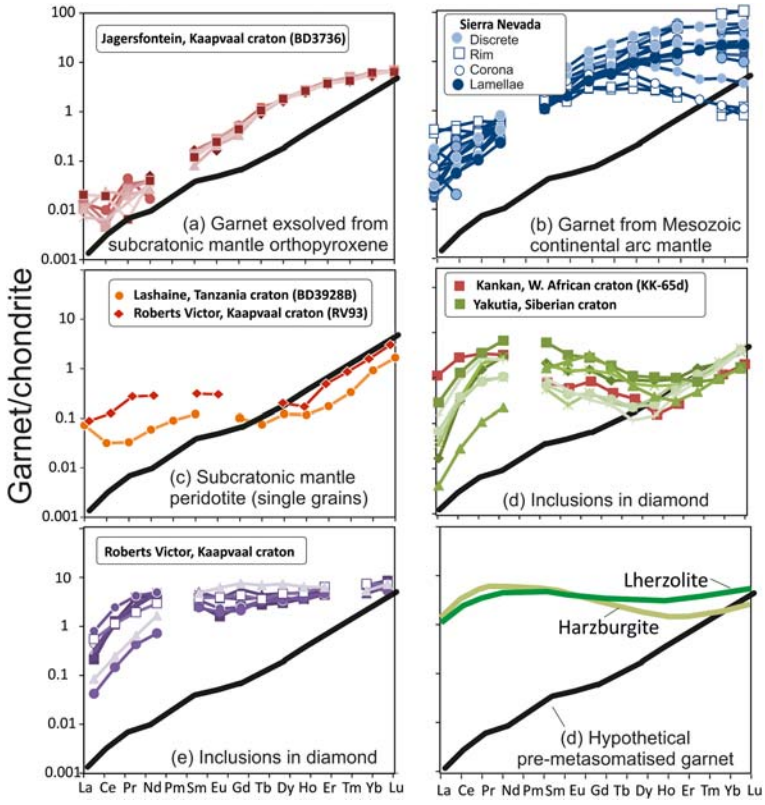

FIG. 11. Comparison of chondrite-normalized rare-earth element (*REE*) patterns for garnets: (*a*) exsolved in Kaapvaal orthopyroxene megacryst BD3636/1 with: (*b*) from Sierra Nevada peridotites (Chin *et al.*, 2012); (*c*) with ultra-depleted CaO contents found at Lashaine, Tanzania (Gibson *et al.*, 2013); (*d*) and (*e*) present in peridotitic diamond inclusions from Kankan, Yakutia and Roberts Victor mine (Stachel *et al.*, 1998, 2000; Taylor *et al.*, 2003); and (*f*) with *REE* patterns akin to those typical of lherzolite and harzburgite paragenesis (Stachel and Harris, 2008). The former have flat middle-to-heavy *REE* patterns while the latter are distinguished by their sinusoidal patterns.

The 'normal' *REE* patterns of lherzolitic garnets resemble those generated in experiments on primitive mantle melts (e.g. Tuff and Gibson, 2006; Fig. 11*f*) and are commonly associated with melt-related mantle metasomatism, whereas the sinusoidal *REE* patterns are similar to those of harzburgitic garnets that are thought to result from the infiltration of low-temperature fluids (Stachel *et al.*, 1998; Stachel and Harris, 1997) or carbonatitic melts (Shu and Brey, 2015). An interesting paradox arises from the fact that while all of the exsolved garnets have a lherzolitic affinity in terms of their CaO and Cr_2O_3 contents (Fig. 2) some of their *REE* patterns resemble those found in mantle harzburgites (Fig. 11*f*). This dichotomy most likely arises because the *REE*s are incorporated in garnet via exchange with divalent cations that occupy the eight-fold site other than simply Ca (e.g. Mg; Orman *et al.*, 2002). Also, garnet has high partition coefficients for many incompatible trace elements, relative to olivine and orthopyroxene, and numerical models show that only a small percentage of fluid or melt is required to change the *REE* pattern from strongly *LREE*-depleted to 'normal' (Gibson *et al.*, 2013; Shu and Brey, 2015).

Beneath southern Africa, craton-scale metasomatism has been multi-phase (Kramers *et al.*, 1983; Menzies and Murphy, 1980; Shu *et al.*, 2013) and is most prevalent in the lower part (130–200 km) of the Kaapvaal lithosphere, where it is associated with deformed high-temperature peridotites. At shallow depths (<105 km) – and where orthopyroxene megacryst BD3736/1 was entrained – the lithospheric mantle is characterized by coarse,

low-temperature peridotites that contain garnets which have largely escaped metasomatism (Burgess and Harte, 1999, 2004). As only a very small proportion (~5%) of the Kaapvaal lithospheric mantle is formed of harzburgite (Schulze, 1995), and hence has remained immune from chemical over-printing, it is not surprising that incompatible-trace-element-depleted signatures such as those observed in exsolved garnets from BD3736/1 are rare.

In comparison to many of the world's other cratons the lithospheric mantle underlying the eastern and central parts of the Kaapvaal, Tanzanian and northern Siberian cratons is unusually rich in orthopyroxene (Boyd, 1989; Boyd and Mertzman, 1987; Griffin *et al.*, 1999*b*; Rudnick *et al.*, 1994). Of these, the lithospheric mantle beneath the Kaapvaal craton contains the greatest amount of orthopyroxene and is present in almost two-fold the abundance of average Archean cratonic mantle (Table 5). This 'excess' in orthopyroxene (enstatite) occurs at the expense of olivine and requires that the bulk-rock Mg# remains constant but SiO_2 contents are increased. The formation of excess orthopyroxene appears to have taken place prior to or during lithospheric thickening, thermal consolidation and stabilization (i.e. cratonization) at ~2.9 to 2.75 Ga and has been attributed variously to: (1) extraction of komatiite melts in the Archean (Boyd, 1989; Doucet *et al.*, 2012); (2) crystallization from an SiO_2-rich ultrabasic magma (Herzberg, 1993); (3) phase transformation from olivine to orthopyroxene by reaction with percolating silicic fluids, rich in Al, Ca and Na (Kelemen *et al.*, 1998; Kesson and Ringwood, 1989; Rudnick *et al.*, 1994):

$$[MgFe]_2SiO_4 + SiO_2 \rightarrow [MgFe]_2Si_2O_6.$$

The high Mg# of many of the pre-cursor orthopyroxenes is consistent with their formation as either a residue of mantle melting or a reaction product of a silicic fluid with Fo-rich olivine, rather than crystal fractionation from a more Fe-rich kimberlite host.

Control of orthopyroxene composition and subsolidus cooling on garnet exsolution

In the Kaapvaal orthopyroxenes studied here there is no correlation between either the style of garnet exsolution or presence/absence of Cr-diopside with temperature or pressure. This suggests that their formation is dependent upon the composition of the host orthopyroxene and consistent with the findings of Canil (1991), which showed that the ability of orthopyroxene (enstatite) to exsolve pyrope garnet and/or Cr-diopside during sub-solidus cooling of the mantle is dependent upon Al_2O_3 and CaO contents. Concentrations of these oxides vary systematically in orthopyroxenes that formed as melt residues in different tectonic settings (see Gibson *et al.*, 2008 and Fig. 7): those in garnet harzburgites from on-craton settings usually have a restricted range of Al_2O_3 (<1 wt.%) and CaO (0.5 wt.%) whereas orthopyroxenes in spinel harzburgites from off-craton and oceanic settings exhibit a much wider positive correlation between Al_2O_3 (up to 6 wt.%) and CaO (up to 2 wt.%). Figure 7 shows that most of the recalculated, bulk pre-exsolution compositions of Kaapvaal orthopyroxenes are characterized by high Al_2O_3 relative to typical cratonic orthopyroxene and plot in the field of spinel-bearing off-craton or abyssal peridotites. Exceptions are the recalculated, pre-exsolution compositions of orthopyroxene megacrysts from Frank Smith mine which have very high CaO but low Al_2O_3 contents; in this respect they are similar to orthopyroxenes found in metasomatized and sheared, high-temperature garnet peridotites (lherzolites, Fig. 7).

The high Mg# (91–94) estimated for the pre-exsolution orthopyroxenes (except those from Frank Smith mine) are characteristic of those found in depleted harzburgites, which are thought to have formed as residues of a large amount of upwelling and adiabatic decompression melting (Boyd *et al.*, 1993; Harte, 1983; O'Hara *et al.*, 1975). If reaction of olivine with silicic fluids was also involved in the formation of the orthopyroxene this would require highly-forsteritic olivine to transform to high-Mg# orthopyroxene. While the orthopyroxenes show no geochemical evidence for this process it might offer a plausible explanation for the large size of the orthopyroxene crystals. Regardless of this uncertainty, the large amounts of decompression melting required to explain the high Mg# of the pre-exsolution orthopyroxenes (Herzberg, 2004) imply that they are associated with residues that formed as a consequence of large amounts of melting at relatively low pressures (<2.5 GPa) in the melting regime, i.e. at significantly lower pressures than those at which the orthopyroxenes exhibiting garnet exsolution equilibrated in the lithospheric mantle prior to their entrainment (Table 4). Although at shallow pressures the stable Al-bearing mantle phase would be spinel (Fig. 10) it is unlikely that this would exist in the residue at such high degrees of melting.

The dominant control on diffusion and subsolidus exsolution is temperature. While there remains a lack of consensus as to the processes involved in cratonization (e.g. Arndt *et al.*, 2009; Aulbach, 2012; Pearson and Wittig, 2008) it seems plausible that the coarse exsolution textures in the orthopyroxenes correspond to slow cooling, from near-anhydrous peridotite solidus conditions in the Archean to those of the present-day sub-cratonic conductive geotherm. The final recorded equilibration temperatures of the orthopyroxenes are well below that of their formation (Table 4), as either a melt residue or reaction product of olivine with silicic fluids prior to cratonization (i.e. >2.5 Ga). Beneath the cratons the gradient of the conductive geotherm (i.e. dP/dT) is smaller than that of the anhydrous peridotite solidus so that the subsolidus cooling interval (ΔT) varies with pressure (Fig. 10):

$$\Delta T\ (^{\circ}\mathrm{C}) = T_{\text{anhydrous solidus}} - T_{\text{conductive geotherm}}.$$

On the basis of a conductive geotherm of 45.6 mW/m^2 for the Kaapvaal craton, ΔT corresponds to ~700°C at a pressure of 2.5 GPa and decreases to 500°C at 4.5 GPa (Fig. 10). The experiments of Canil (1991) indicate that, under these circumstances, garnet would start to exsolve from orthopyroxene at ~200°C below the solidus. Diffusion of Ca^{2+}, Al^{3+} and Si^{4+} from the orthopyroxene lattice below this temperature would continue to the final cooling temperature defined by the conductive geotherm, i.e. over a temperature interval of <500°C. The ΔT calculations shown in Table 4 assume that the exsolution process is isobaric, which is a simplified approach as garnet would almost certainly be exsolving over a range of pressures. Even with this assumption it is not straight forward to calculate the amount of time for garnet to form thick lamellae in mantle orthopyroxenes. This is because: (1) the diffusion rate of Al in orthopyroxene is poorly constrained (Chin *et al.*, 2015); and (2) the cooling rate of cratonic lithosphere – since its time of isolation from the convecting mantle and subsequent stabilisation >2.5 Ga – is poorly known. Estimates from isotopic studies of mantle xenoliths and geophysical investigations for cooling of the cratonic lithosphere range from 0.04 to 0.1°C/Ma (Bedini *et al.*, 2004; Michaut and Jaupart, 2007; Shu *et al.*, 2014). Such a slow cooling rate would readily explain the sub-solidus exsolution of garnet from orthopyroxene during the last 2.5 Ga, over the 500 to 700°C interval between the dry peridotite solidus. Nevertheless, the occurrence of garnet lamellae in mantle orthopyroxene from much younger terranes indicates that this process may be much faster (see below).

Is the Sierra Nevada continental arc (western USA) a Mesozoic analogue for garnet exsolution in thickened Archean lithosphere?

The mechanisms that occurred during the exsolution of garnet in orthopyroxenes from the Kaapvaal craton are unclear but may be similar to those recently inferred from peridotite xenoliths from the Late Mesozoic Sierra Nevada continental arc in California (Chin *et al.*, 2012, 2015). The Sierra Nevada garnets occur as rods and lamellae in orthopyroxene as well as discrete grains and coronas around spinel. The width of the exsolved rods and lamellae ranges from 100 nm to 30 μm, and therefore at a much-finer length scale than observed in the Kaapvaal orthopyroxenes described above. Both the exsolved and discrete Sierra Nevada garnets have similar CaO (4 to 5.5 wt.%) but slightly lower Cr_2O_3 contents (1 to 2 wt.%) than the exsolved Kaapvaal garnets, and are also 'lherzolitic' (Fig. 2). The Sierra Nevada garnets are, however, less magnesian (Mg# = 75–80) than the exsolved Kaapvaal garnets (Mg# = 63–87) and have elevated concentrations of *REE*s (*HREE*s are up to ~50 × chondrite, Fig. 11*b*). The most *LREE* depleted analyses of Sierra Nevada garnets are from the cores of discrete grains and exsolved lamellae, and their overall *REE* patterns resemble the strongly *LREE* depleted garnets exsolved in Kaapvaal orthopyroxene megacryst BD3736/1 (Fig. 11*a*). In contrast to the Kaapvaal samples, some Sierra Nevada garnets are not fully equilibrated and their rims exhibit mildly-sinusoidal patterns that are similar to some Kaapvaal megacrysts (e.g. BD2015/5, Table 3).

The lower temperatures of the convecting mantle in the Mesozoic compared to the Archean would decrease the depth and amount of partial melting of upwelling peridotite. This may well explain the generally lower Mg# of Sierra Nevada host orthopyroxenes (mean Mg# = 91.5) and their exsolved garnets. The higher Mg# of the Kaapvaal orthopyroxenes (mean Mg# = 92.6, excl. Frank Smith mine) may account for their lower *REE* concentrations as the *REE*s are thought to partially substitute for Mg in garnet (Orman *et al.*, 2002). The sinusoidal *REE* patterns displayed by the rims of some of the Sierran garnets

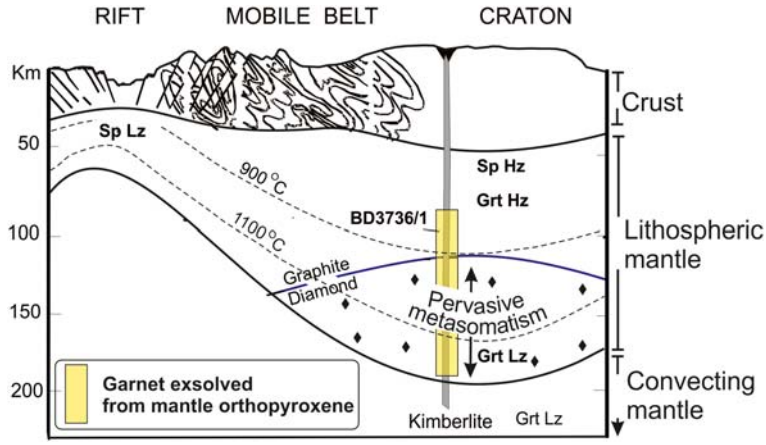

FIG. 12. Schematic illustration of the lithospheric mantle beneath the Kaapvaal craton, highlighting the large depth interval (90 km) over which garnet has exsolved from orthopyroxene. The thickness of the lithosphere (mechanical boundary layer) beneath the Kaapvaal craton is taken from the conductive geotherm calculated for Finsch mine (see Fig. 10). The graphite-diamond stability field is from Kennedy and Kennedy (1976). Mantle metasomatism is pervasive in the lowermost (~75 km) of the lithosphere.

and also garnet coronas around spinel may be linked to a refertilization event immediately prior to entrainment (Chin *et al.*, 2012). Such disequilibrium is not evident in the exsolved Kaapvaal garnets but the sinusoidal and normal *REE* patterns of some of these garnets may be testimony to a refertilization event well before the time of entrainment.

Akin to the model proposed above for the Kaapvaal samples, Chin *et al.* (2012) suggested that the protoliths of the Sierra Nevada garnet-bearing peridotites were spinel peridotites, formed by shallow melt depletion (1–2 GPa, 1300–1400°C) followed by compression and cooling in the garnet stability field, as a consequence of progressive thickening of the Sierran arc lithosphere. Chin *et al.* (2015) modelled Al-diffusion profiles in the orthopyroxenes and combined these with Lu-Hf and Sm-Nd model ages to show that the Sierran lithosphere cooled very quickly (<10 M.y.) from 1250 to 750°C, just after the peak of arc magmatism. One possible scenario is that the isochemical subsolidus exsolution of garnet from orthopyroxene in sub-cratonic mantle occurred during cratonization and rapid lithospheric thickening at ~2.5 Ga. A detailed Sm-Nd and Lu-Hf isotopic investigation is now required to date closure temperatures for the exsolved clinopyroxene and garnet (see Shu *et al.*, 2014). These timescales of exsolution could potentially distinguish between the different processes that have been proposed for the formation of cratonic lithosphere, i.e. evidence of rapid cooling would be consistent with models that invoke tectonic thickening whereas conductive cooling of a thermal boundary layer would require longer timescales.

Conclusions

(1) Orthopyroxenes (enstatite) found as megacrysts and also in mantle xenoliths entrained in kimberlites from southern parts of the Kaapvaal craton show evidence for isochemical exsolution of pyrope garnet and in some cases Cr-diopside. Spectacular microstructures formed by exsolved garnet vary from fine to coarse lamellae and are best preserved in orthopyroxene megacrysts. The diffusion length scale of garnet forming coarse lamellae in large (20 mm) orthopyroxene megacrysts is 2 mm. For smaller orthopyroxene grains (<10 mm), found in peridotite xenoliths, diffusion lengths of Ca^{2+}, Al^{3+} and Si^{4+} are such that garnet nucleates on orthopyroxene grain boundaries. These are most readily identified when they form interconnected networks or 'necklace' textures. They may also form discrete grains but establishing the origin of these is more enigmatic.

(2) Pressure and temperature estimates reveal the orthopyroxenes with exsolved garnet were

entrained from a wide depth interval (85–175 km) that occupies almost the whole of the garnet stability field in the Kaapvaal lithospheric mantle (Fig. 12).

(3) The recalculated compositions of many of the precursor (pre-exsolution) orthopyroxenes are characterized by high Mg#, Al_2O_3 and CaO contents. They resemble residues formed by adiabatic decompression melting in the shallow (spinel-facies) mantle but a reaction involving transformation from olivine by reaction with silica-rich fluids cannot be excluded. The temperatures of initial orthopyroxene formation are significantly higher – and their pressures much less – than those of their final equilibration, and it is proposed that garnet exsolution probably occurred during lithospheric thickening. This may have been during cratonization (i.e. prior to 2.5 Ga) but further work is required to establish the timing of this. Analogous microstructures of garnet exsolution from orthopyroxene are preserved in peridotite mantle xenoliths from the Late Mesozoic Sierra Nevada continental arc. Here, where the tectonic setting is much better understood, and coexisting phases are not yet fully equilibrated, exsolution of garnet from orthopyroxene has been estimated to occur in ~10 M.y., i.e. very rapid (Chin *et al.*, 2015).

(4) Garnets exsolved from orthopyroxenes entrained from the lower parts of the sub-cratonic lithosphere appear to have undergone refertilization by metasomatic melts and fluids but those entrained from much shallower depths (~90 km) are strongly-depleted in *LREE*s and preserve their original isochemical exsolution compositions. This is a significant feature of the dataset because these compositions represent the closest approximation to those proposed for hypothetical pre-metasomatic garnets of any published to date. They provide important end-member compositions in models of enrichment of highly-depleted peridotite in the lithospheric mantle by reactive percolation of fluids and melts, which in some cases involved the synchronous growth of diamond.

(5) The modal abundance of garnet formed by isochemical exsolution from orthopyroxene in the Kaapvaal sub-cratonic mantle and elsewhere is unclear but may prove to be an important consideration in models put forward to explain the widespread occurrence and nature of garnet, and processes involved in the formation and stabilization of Earth's most ancient continental lithospheric mantle.

Acknowledgements

The research presented in this manuscript formed the basis of the 45th Hallimond Lecture at the 50th annual meeting of the *Volcanic and Magmatic Studies Group* (University of Edinburgh, UK). I am sincerely grateful to the *Mineralogical Society* for this award. Research on garnet exsolution was inspired by the late J. Barry Dawson, who was a pioneer in the study of mantle xenoliths and continental magmatism. His extensive field work in Africa, systematic sample collection and incisive interpretations generated a wealth of publications that have greatly aided our understanding of Earth's mantle. I thank Tim Holland and Michael Carpenter for their inspirational discussions on garnet exsolution. Electron microprobe analyses of orthopyroxene megacrysts were carried out by Alex Clarke as part of an MSci project at the University of Cambridge. Technical assistance with analyses of mineral chemistry was provided by Iris Buisman (electron microprobe, QEMSCAN®) and Jason Day (LA-ICP-MS) and I thank them warmly for their sustained support. The clarity of the manuscript was improved by the constructive comments of Yannick Bussweiler and an anonymous reviewer.

References

Aoki, K.-I., Fujimaki, H. and Kitamura, M. (1980). Exsolved garnet-bearing pyroxene megacrysts from some South African kimberlites. *Lithos*, **13**, 269–279.

Arndt, N.T., Coltice, N., Helmstaedt, H. and Gregoire, M. (2009) Origin of Archean subcontinental lithospheric mantle: Some petrological constraints. *Lithos*, **109**, 61–71.

Artemieva, I.M. (2011) *The Lithosphere*. Cambridge University Press, Cambridge, UK.

Aulbach, S. (2012) Craton nucleation and formation of thick lithospheric roots. *Lithos*, **149**, 16–30.

Bedini, R.-M., Blichert-Toft, J., Boyet, M. and Albarède, F. (2004) Isotopic constraints on the cooling of the continental lithosphere. *Earth and Planetary Science Letters*, **223**, 99–111.

Beeson, M.H. and Jackson, E.D. (1970) Origin of garnet pyroxenite xenoliths at Salt Lake crater. *Mineralogical Society of America Special Publication*, **S3**, 95–112.

Begg, G.C., Griffin, W.L., Natapov, L.M., O'Reilly, S.Y., Grand, S.P., O'Niell, C.J., Hronsky, J.M.A., Poudjom Djomani, Y., Swain, C.J., Deen, T. and Bowden, P. (2009) The lithospheric architecture of Africa: Seismic tomography, mantle petrology, and tectonic evolution. *Geosphere*, **5**, 23–50.

Bell, D.R., Schmitz, M.D. and Janney, P.E. (2003) Mesozoic thermal evolution of the southern African mantle lithosphere. *Lithos*, **71**, 273–287.

Boyd, F.R. (1989) Compositional distinction between oceanic and cratonic lithosphere. *Earth and Planetary Science Letters*, **96**, 15–26.

Boyd, F.R. and Mertzman, S.A. (1987) Composition and structure of the Kaapvaal lithosphere, South Africa. Pp. 13–24 in: *Magmatic Processes: Physiochemical Principles* (B.O. Mysen, editor). Geochemical Society Special Publication, **1**.

Boyd, F.R., Pearson, D.G., Nixon, P.H. and Mertzman, S. A. (1993) Low-calcium garnet harzburgites from southern Africa: their relations to craton structure and diamond crystallization. *Contributions to Mineralogy and Petrology*, **113**, 352–366.

Brey, G.P. and Kohler, T. (1990) Geothermobarometry in four-phase lherzolites II. New thermobarometers, and practical assessment of existing thermobarometers. *Journal of Petrology*, **31**, 1353–1378.

Brey, G.P., Kohler, T. and Nickel, K.G. (1990) Geothermobarometry in four-phase lherzolites I. Experimental results from 10 to 60 kb. *Journal of Petrology*, **31**, 1313–1352.

Burgess, S.R. and Harte, B. (1999) Tracing lithosphere evolution through the analysis of heterogeneous G9/ G10 garnets in peridotite xenoliths, I: major element chemistry. *Proceedings of the 7th International Kimberlite Conference*, 66–80.

Burgess, S.R. and Harte, B. (2004) Tracing lithosphere evolution through the analysis of heterogeneous G9–G10 garnets in peridotite xenoliths, II: REE chemistry. *Journal of Petrology*, **45**, 609–633.

Bussweiler, Y., Stone, R.S., Pearson, D.G., Luth, R.W., Stachel, T., Kjarsgaard, B.A. and Menzies, A. (2016) The evolution of calcite-bearing kimberlites by melt-rock reaction: evidence from polymineralic inclusions within clinopyroxene and garnet megacrysts from Lac de Gras kimberlites, Canada. *Contributions to Mineralogy and Petrology*, **171**, 65.

Canil, D. (1991) Experimental evidence for the exsolution of cratonic peridotite from high-temperature harzburgite. *Earth and Planetary Science Letters*, **106**, 64–72.

Carlson, R.W., Pearson, D.G. and James, D.E. (2005) Physical, chemical, and chronological characteristics of continental mantle. *Reviews of Geophysics*, **43**, https://doi.org:10.1029/2004RG000156.

Chin, E.J., Lee, C.-T.A. and Blichert-Toft, J. (2015) Growth of upper plate lithosphere controls tempo of arc magmatism: Constraints from Al-diffusion kinetics and coupled Lu-Hf and Sm-Nd chronology. *Geochemical Perspectives Letters*, **1**, 20–32.

Chin, E.J., Lee, C.-T.A., Luffi, P. and Tice, M. (2012) Deep lithospheric thickening and refertilization beneath continental arcs: Case Study of the P, T and compositional evolution of peridotite xenoliths from the Sierra Nevada, California. *Journal of Petrology*, **53**, 477–511.

Dawson, J.B. (1981) The nature of the upper mantle. *Mineralogical Magazine*, **44**, 1–18.

Dawson, J.B. (1987) Metasomatised harzburgites in kimberlite and alkaline magmas: enriched restites and "flushed" lherzolites. Pp. 125–144 in: *Mantle metasomatism* (M.A. Menzies and C.J. Hawkesworth, editors). Academic Press, London.

Dawson, J.B. (2004) A fertile harzburgite-garnet lherzolite transition: possible inferences for the roles of strain and metasomatism in upper mantle peridotites. *Lithos*, **77**, 553–569.

Dawson, J.B., Smith, J.V. and Hervig, R.L. (1980) Heterogeneity in upper-mantle lherzolites and harzburgites. *Philosophical Transactions of the Royal Society of London. Series A, Mathematical and Physical Sciences*, **297**, 323–332.

Dawson, P.J.B. (1980) The Megacryst Suite. Pp. 190–199 in: *Kimberlites and Their Xenoliths*. Springer, Berlin-Heidelberg,

Doucet, L.S., Ionov, D.A., Golovin, A.V. and Pokhilenko, N.P. (2012) Depth, degrees and tectonic settings of mantle melting during craton formation: inferences from major and trace element compositions of spinel harzburgite xenoliths from the Udachnaya kimberlite, central Siberia. *Earth and Planetary Science Letters*, **359–360**, 206–218.

Eggler, D.H., McCallum, M.E.H. and Smith, C.B. (1979) Megacryst assemblages in kimberlite from Northern Colorado and Southern Wyoming: Petrology, geothermometry-barometry, and areal distribution. Pp. 213–226 in: *The Mantle Sample: Inclusion in Kimberlites and Other Volcanics* (H.O.A. Meyer and F.R. Boyd, editors). American Geophysical Union, USA.

Eggler, D.H. and Wendlandt, R.F. (1982) Experimental studies on the relationship between kimberlite magmas and partial melting of peridotite. Pp. 330–338 in: *Kimberlites, Diatremes, and Diamonds: Their Geology, Petrology, and Geochemistry* (H.O.A. Meyer and F.R. Boyd, editors). American Geophysical Union, USA.

Faryad, S.W., Dolejš, D. and Machek, M. (2009) Garnet exsolution in pyroxene from clinopyroxenites in the Moldanubian zone: constraining the early pre-convergence history of ultramafic rocks in the Variscan orogen. *Journal of Metamorphic Geology*, **27**, 655–671.

Gibson, S.A., Malarkey, J. and Day, J.A. (2008) Melt depletion and enrichment beneath the Western Kaapvaal Craton: Evidence from Finsch peridotite xenoliths. *Journal of Petrology*, **49**, 1817–1852.

Gibson, S.A., McMahon, S.C., Day, J.A. and Dawson, J. B. (2013) Highly-refractory lithospheric mantle beneath the Tanzanian Craton: evidence from Lashaine pre-metasomatic garnet-bearing peridotites. *Journal of Petrology*, **54**, 1503–1546.

Griffin, W.L., Fisher, N.I., Friedman, J., Ryan, C.G. and O'Reilly, S.Y. (1999*a*) Cr-pyrope garnets in the lithospheric mantle. I. Compositional systematics and relations to tectonic setting. *Journal of Petrology*, **40**, 679–704.

Griffin, W., O'Reilly, S. and Ryan, C. (1999*b*) The composition and origin of sub-continental lithospheric mantle. Pp. 13–45 in: *Mantle Petrology: Field Observations and High-Pressure Experimentation: A Tribute To Francis R.(Joe) Boyd*. The Geochemical Society Houston, USA.

Griffin, W.L., O'Reilly, S.Y., Natapov, L.M. and Ryan, C. G. (2003) The evolution of lithospheric mantle beneath the Kalahari Craton and its margins. *Lithos*, **71**, 215–241.

Grütter, H.S. and Tuer, J. (2009) Constraints on deep mantle tenor of Sarfartoq-area kimberlites (Greenland), based on modern thermobarometry of mantle-derived xenocrysts. *Lithos*, **112**, [Supplement 1], 124–129.

Grütter, H.S., Apter, D.B. and Kong, J. (1999) Crust-mantle coupling: evidence fom mantle-derived xenocrystic garnets. *Proceedings of 7th International Kimberlite Conference*, 307–313.

Grütter, H.S., Gurney, J.J., Menzies, A.H. and Winter, F. (2004) An updated classification scheme for mantle-derived garnet, for use by diamond explorers. *Lithos*, **77**, 841–857.

Gurney, J.J. and Switzer, G.S. (1973) The discovery of garnets closely related to diamonds in the Finsch pipe, South Africa. *Contributions to Mineralogy and Petrology*, **39**, 103–116.

Gurney, J.J., Jakob, W.R.O. and Dawson, J.B. (1979) Megacrysts from the Monastery Kimberlite Pipe, South Africa. Pp. 227–243 in: *The Mantle Sample: Inclusion in Kimberlites and Other Volcanics* (F.R. Boyd, and H.O.A. Meyer, editors). American Geophysical Union, USA.

Harte, B. (1983) Mantle peridotites and processes – the kimberlite sample. Pp. 46–91 in: *Continental Basalts and Mantle Xenoliths* (C.J. Hawkesworth and M.J. Norry, editors) Shiva, Nantwich, UK.

Harte, B. and Gurney, J.J. (1975) Evolution of clinopyroxene and garnet in an eclogite nodule from the Roberts Victor kimberlite pipe, South Africa. *Physics and Chemistry of the Earth*, **9**, 367–387.

Harte, B. and Gurney, J.J. (1981) The mode of formation of chromium-poor megacryst suites from kimberlites. *The Journal of Geology*, **89**, 749–753.

Harte, B., Hunter, R.H. and Kinny, P.D. (1993) Melt geometry, movement and crystallization, in relation to mantle dykes, veins and metasomatism. *Philosophical Transactions of the Royal Society of London A: Mathematical, Physical and Engineering Sciences*, **342**, 1–21.

Herzberg, C. (1993) Lithosphere peridotites of the Kaapvaal craton. *Earth and Planetary Science Letters*, **120**, 13–29.

Herzberg, C. (2004) Geodynamic information in peridotite petrology. *Journal of Petrology*, **45**, 2507–2530.

Herzberg, C. and Rudnick, R. (2012) Formation of cratonic lithosphere: An integrated thermal and petrological model. *Lithos*, **149**, 4–15.

Hirschmann, M.M. (2000) Mantle solidus: Experimental constraints and the effects of peridotite composition. *Geochemistry Geophysics Geosystems*, **1**, 26 PP.

Ivanic, T.J., Harte, B. and Gurney, J.J. (2016) A discussion of "Mineralogical controls on garnet composition in the cratonic mantle" by Hill *et al.*, Contributions to Mineralogy and Petrology (2015) 169:13. *Contributions to Mineralogy and Petrology*, **171**, 1–4.

Jerde, E.A., Taylor, L.A., Crozaz, G. and Sobolev, N.V. (1993) Exsolution of garnet within clinopyroxene of mantle eclogites: major- and trace-element chemistry. *Contributions to Mineralogy and Petrology*, **114**, 148–159.

Johnson, K.T.M. (1998) Experimental determination of partition coefficients for rare earth and high-field-strength elements between clinopyroxene, garnet, and basaltic melt at high pressures. *Contributions to Mineralogy and Petrology*, **133**, 60–68.

Jordan, T.H. (1979) Mineralogies, densities and seismic velocities of garnet lherzolites and their geophysical implications. Pp. 1–14 in: *The Mantle Sample: Inclusions in Kimberlites and Other Volcanics* (F.R. Boyd and H.O. Meyer, editors). Proceedings of the 2nd International Kimberlite Conference, AGU, Washington D.C.

Kelemen, P.B., Hart, S. and Bernstein, S. (1998) Silica enrichment in the continental upper mantle via melt/rock reaction. *Earth and Planetary Science Letters*, **164**, 387–406.

Kennedy, C.S. and Kennedy, G.C. (1976) The equilibrium boundary between graphite and diamond. *Journal of Geophysical Research*, **81**, 2467–2470.

Kesson, S.E. and Ringwood, A.E. (1989) Slab-mantle interactions: 2. The formation of diamonds. *Chemical Geology*, **78**, 97–118.

Klemme, S. and O'Neill, H.S.C., (2000) The near-solidus transition from garnet lherzolite to spinel lherzolite. *Contributions to Mineralogy and Petrology*, **138**, 237–248.

Kramers, J.D., Roddick, J.C.M. and Dawson, J.B. (1983) Trace element and isotope studies on veined, metasomatic and "MARID" xenoliths from Bultfontein, South Africa. *Earth and Planetary Science Letters*, **65**, 90–106.

Lazarov, M., Woodland, A.B. and Brey, G.P. (2009) Thermal state and redox conditions of the Kaapvaal mantle: A study of xenoliths from the

Finsch mine, South Africa. *Lithos*, **112** [Supplement 2], 913–923.

Lazarov, M., Brey, G.P. and Weyer, S. (2012) Evolution of the South African mantle – a case study of garnet peridotites from the Finsch diamond mine (Kaapvaal craton); Part 2: Multiple depletion and re-enrichment processes. *Lithos*, **154**, 210–223.

Lee, C.-T.A. and Chin, E.J. (2014) Calculating melting temperatures and pressures of peridotite protoliths: Implications for the origin of cratonic mantle. *Earth and Planetary Science Letters*, **403**, 273–286.

Lee, C.-T., Luffi, P. and Chin, E.J. (2011) Building and destroying continental mantle. *Annual Review of Earth and Planetary Sciences*, **39**, 59–90.

Mather, K.A., Pearson, D.G., McKenzie, D., Kjarsgaard, B.A. and Priestley, K. (2011) Constraints on the depth and thermal history of cratonic lithosphere from peridotite xenoliths, xenocrysts and seismology. *Lithos*, **125**, 729–742.

McDonough, W. and Sun, S.-s. (1995) The composition of the Earth. *Chemical Geology*, **120**, 223–253.

McKenzie, D., Jackson, J. and Priestley, K. (2005) Thermal structure of oceanic and continental lithosphere. *Earth and Planetary Science Letters*, **233**, 337–349.

Menzies, M. and Murphy, V.R. (1980) Enriched mantle: Nd and Sr isotopes in diopsides from kimberlite nodules. *Nature*, **283**, 634–636.

Michaut, C. and Jaupart, C. (2007) Secular cooling and thermal structure of continental lithosphere. *Earth and Planetary Science Letters*, **257**, 83–96.

Moore, A. and Costin, G. (2016) Kimberlitic olivines derived from the Cr-poor and Cr-rich megacryst suites. *Lithos*, **258–259**, 215–227.

Nair, S.K., Gao, S.S., Liu, K.H. and Silver, P.G. (2006) Southern African crustal evolution and composition: Constraints from receiver function studies. *Journal of Geophysical Research: Solid Earth*, **111**, B02304.

Nickel, K.G. and Green, D.H. (1985) Empirical geothermobarometry for garnet peridotites and implications for the nature of the lithosphere, kimberlites and diamonds. *Earth and Planetary Science Letters*, **73**, 158–170.

Nimis, P. and Grütter, H. (2009) Internally consistent geothermometers for garnet peridotites and pyroxenites. *Contributions to Mineralogy and Petrology*, **159**, 411–427.

O'Hara, M.J., Saunders, M.J. and Mercy, E.L.P. (1975) Garnet-peridotite, primary ultrabasic magma and eclogite; Interpretation of upper mantle processes in kimberlite. *Physics and Chemistry of the Earth*, **9**, 571–604.

Orman, J.A.V., Grove, T.L., Shimizu, N. and Layne, G.D. (2002) Rare earth element diffusion in a natural pyrope single crystal at 2.8 GPa. *Contributions to Mineralogy and Petrology*, **142**, 416–424.

Pearson, D.G. and Wittig, N. (2008) Formation of Archaean continental lithosphere and its diamonds: the root of the problem. *Journal of the Geological Society*, **165**, 895–914.

Pearson, D.G. and Wittig, N. (2013) The formation and evolution of cratonic mantle lithosphere – Evidence from mantle xenoliths. Pp. 255–292 in: *The Mantle and Core* (R.W. Carlson, editor). Treatise in Geochemistry, Vol. 3. Elsevier.

Pearson, D.G., Carlson, R.W., Shirey, S.B., Boyd, F.R. and Nixon, P.H. (1995) Stabilisation of Archaean lithospheric mantle: A Re-Os isotope study of peridotite xenoliths from the Kaapvaal craton. *Earth and Planetary Science Letters*, **134**, 341–357.

Pearson, D.G. Brenker, F.E., Nestola, F., McNeill, J., Nasdala, L., Hutchison, M.T., Matveev, S., Mather, K., Silversmit, G., Schmitz, S., Vekemans, B., and Vincze, L. (2014) Hydrous mantle transition zone indicated by ringwoodite included within diamond. *Nature*, **507**, 221–224.

Peslier, A.H., Woodland, A.B., Bell, D.R. and Lazarov, M. (2010) Olivine water contents in the continental lithosphere and the longevity of cratons. *Nature*, **467**, 78–81.

Priestley, K. and McKenzie, D. (2013) The relationship between shear wave velocity, temperature, attenuation and viscosity in the shallow part of the mantle. *Earth and Planetary Science Letters*, **381**, 78–91.

Richter, F.M. (1988) A major change in the thermal state of the Earth at the Archean-Proterozoic boundary: Consequences for the nature and preservation of continental lithosphere. *Journal of Petrology* [Special Lithosphere Issue], 39–52.

Roach, I.C. (2004) Mineralogy, textures and P–T relationships of a suite of xenoliths from the Monaro Volcanic Province, New South Wales, Australia. *Journal of Petrology*, **45**, 739–758.

Rudnick, R.L., McDonough, W.F. and Orpin, A. (1994) Northern Tanzania peridotite xenoliths: a comparison with Kaapvaal xenoliths and inferences of metasomatic reactions. Pp. 336–353 in: *Kimberlites, Related Rocks and Mantle Xenoliths* (H.O.A. Meyer, and O.H. Leonardos, editors). Proceedings 5th International Kimberlite Conference.

Russell, J.K., Porritt, L.A., Lavallée, Y. and Dingwell, D. B. (2012) Kimberlite ascent by assimilation-fuelled buoyancy. *Nature*, **481**, 352–356.

Sautter, V. and Harte, B. (1988) Diffusion gradients in an eclogite xenolith from the Roberts Victor Kimberlite Pipe: 1. Mechanism and evolution of garnet exsolution in Al_2O_3-rich clinopyroxene. *Journal of Petrology*, **29**, 1325–1352.

Sautter, V. and Harte, B. (1990) Diffusion gradients in an eclogite xenolith from the Roberts Victor kimberlite pipe: (2) kinetics and implications for petrogenesis.

Contributions to Mineralogy and Petrology, **105**, 637–649.

Schulze, D.J. (1995) Low-Ca garnet harzburgites from Kimberley, South Africa: Abundance and bearing on the structure and evolution of the lithosphere. *Journal of Geophysical Research: Solid Earth*, **100**, 12513–12526.

Schutt, D.L. and Lesher, C.E. (2010) Compositional trends among Kaapvaal Craton garnet peridotite xenoliths and their effects on seismic velocity and density. *Earth and Planetary Science Letters*, **300**, 367–373.

Shu, Q. and Brey, G.P. (2015) Ancient mantle metasomatism recorded in subcalcic garnet xenocrysts: Temporal links between mantle metasomatism, diamond growth and crustal tectonomagmatism. *Earth and Planetary Science Letters*, **418**, 27–39.

Shu, Q., Brey, G.P., Gerdes, A. and Hoefer, H.E. (2013) Geochronological and geochemical constraints on the formation and evolution of the mantle underneath the Kaapvaal craton: Lu–Hf and Sm–Nd systematics of subcalcic garnets from highly depleted peridotites. *Geochimica et Cosmochimica Acta*, **113**, 1–20.

Shu, Q., Brey, G.P., Gerdes, A. and Hoefer, H.E. (2014) Mantle eclogites and garnet pyroxenites – the meaning of two-point isochrons, Sm–Nd and Lu–Hf closure temperatures and the cooling of the subcratonic mantle. *Earth and Planetary Science Letters*, **389**, 143–154.

Simon, N.S.C., Carlson, R.W., Pearson, D.G. and Davies, G.R. (2007) The origin and evolution of the Kaapvaal cratonic lithospheric mantle. *Journal of Petrology*, **48**, 589–625.

Simon, N.S.C., Irvine, G.J., Davies, G.R., Pearson, D.G. and Carlson, R.W. (2003) The origin of garnet and clinopyroxene in "depleted" Kaapvaal peridotites. *Lithos*, **71**, 289–322.

Smith, C.B., Gurney, J.J., Skinner, E.M.W., Clement, C.R. and Ebrahim, N. (1985) Geochemical character of Southern African kimberlites; a new approach based on isotopic constraints. *South African Journal of Geology*, **88**, 267–280.

Sobolev, N.V., Lavrent'ev, Y.G., Pokhilenko, N.P. and Usova, L.V. (1973) Chrome-rich garnets from the kimberlites of yakutia and their parageneses. *Contributions to Mineralogy and Petrology*, **40**, 39–52.

Soltys, A., Giuliani, A., Phillips, D., Kamenetsky, V.S., Maas, R., Woodhead, J. and Rodemann, T. (2016) In-situ assimilation of mantle minerals by kimberlitic magmas – Direct evidence from a garnet wehrlite xenolith entrained in the Bultfontein kimberlite (Kimberley, South Africa). *Lithos*, **256–257**, 182–196.

Stachel, T., Brey, G.P. and Harris, J.W. (2000) Kankan diamonds (Guinea) I: from the lithosphere down to the transition zone. *Contributions to Mineralogy and Petrology*, **140**, 1–15.

Stachel, T., Aulbach, S., Brey, G.P., Harris, J.W., Leost, I., Tappert, R. and Viljoen, K.S. (2004) The trace element composition of silicate inclusions in diamonds: a review. *Lithos*, **77**, 1–19.

Stachel, T., Brey, G.P. and Harris, J.W. (2005) Inclusions in sublithospheric diamonds: Glimpses of deep Earth. *Elements*, **1**, 73–78.

Stachel, T. and Harris, J.W. (1997) Diamond precipitation and mantle metasomatism – evidence from the trace element chemistry of silicate inclusions in diamonds from Akwatia, Ghana. *Contributions to Mineralogy and Petrology*, **129**, 143–154.

Stachel, T. and Harris, J.W. (2008) The origin of cratonic diamonds – Constraints from mineral inclusions. *Ore Geology Reviews*, **34**, 5–32.

Stachel, T., Viljoen, K.S., Brey, G. and Harris, J.W. (1998) Metasomatic processes in lherzolitic and harzburgitic domains of diamondiferous lithospheric mantle: REE in garnets from xenoliths and inclusions in diamonds. *Earth and Planetary Science Letters*, **159**, 1–12.

Stephens, W.E. and Dawson, J.B. (1977) Statistical comparison between pyroxenes from kimberlites and their associated xenoliths. *The Journal of Geology*, **85**, 433–449.

Taylor, L.A., Anand, M., Promprated, P., Floss, C. and Sobolev, N.V. (2003) The significance of mineral inclusions in large diamonds from Yakutia, Russia. *American Mineralogist*, **88**, 912–920.

Taylor, W.R. (1998) An experimental test of some geothermometer and geobarometer formulations for upper mantle peridotites with application to the thermobarometry of fertile lherzolite and garnet websterite. *Neues Jahrbuch Fur Mineralogie Abhandlungen*, **172**, 381–408.

Tuff, J. and Gibson, S.A. (2006) Trace-element partitioning between garnet, clinopyroxene and Fe-rich picritic melts at 3 to 7 GPa. *Contributions to Mineralogy and Petrology*, **153**, 369–387.

von Seckendorff, V. and O'Neill, H.S.C. (1993) An experimental study of Fe-Mg partitioning between olivine and orthopyroxene at 1173, 1273 and 1423 K and 1.6 GPa. *Contributions to Mineralogy and Petrology*, **113**, 196–207.

Walker, R.J., Carlson, R.W., Shirey, S.B. and Boyd, F.R. (1989) Os, Sr, Nd, and Pb isotope systematics of southern African peridotite xenoliths: Implications for the chemical evolution of subcontinental mantle. *Geochimica et Cosmochimica Acta*, **53**, 1583–1595.

Walter, M.J. (1998) Melting of garnet peridotite and the origin of komatiite and depleted lithosphere. *Journal of Petrology*, **39**, 29–60.

Walter, M.J., Kohn, S.C., Araujo, D., Bulanova, G.P., Smith, C.B., Gaillou, E., Wang, J., Steele, A. and Shirey, S.B. (2011) Deep mantle cycling of oceanic

crust: Evidence from diamonds and their mineral inclusions. *Science*, **334**, 54–57.

Wilkinson, J.F.G. (1976) Some subcalcic clinopyroxenites from Salt Lake Crater, Oahu, and their petrogenetic significance. *Contributions to Mineralogy and Petrology*, **58**, 181–201.

Ziberna, L., Nimis, P., Zanetti, A., Marzoli, A. and Sobolev, N.V. (2013) Metasomatic processes in the central Siberian cratonic mantle: Evidence from garnet xenocrysts from the Zagadochnaya kimberlite. *Journal of Petrology*, **54**, 2379–2409.